Chapter 3
Nonlinear Oscillator and a Non-ideal Energy Source

In this chapter the motion of the non-ideal system which contains a nonlinear one degree-of-freedom oscillator and a non-ideal energy source is considered. In such a non-ideal oscillator-motor system there is an interaction between motions of the oscillator and of the motor as it was already explained in the previous chapter. However, due to nonlinear properties of the oscillator in the non-ideal system beside the Sommerfeld effect some additional phenomena are evident. Depending on the parameter properties of the oscillator the motion is regular or irregular. Results on motion of the non-ideal systems with nonlinear oscillators are published in Dimentberg et al. (1997), Warminski et al. (2001), Warminski and Kecik (2006) Dantas and Balthazar (2007), Felix et al. (2009a), Zukovic and Cveticanin (2007, 2009), Nbendjo et al. (2012), Cveticanin and Zukovic (2015a, b) etc.

This chapter is divided into five sections. In Sect. 3.1, a generalization of the model of the non-ideal oscillator-motor is done: a strong nonlinear oscillator is coupled with a motor with nonlinear torque property. The model of the structure-motor system is generalized by assuming that the driving torque is a nonlinear function of the angular velocity and the oscillator is with strong nonlinearity. The oscillator-motor system is assumed as a non-ideal one where not only the motor affects the motion of the oscillator but also vibrations of the oscillator have an influence on the motor motion. The model of the motor-structure system is described with two coupled strong nonlinear differential equations. An improved asymptotic analytic method based on the averaging procedure is developed for solving such a system of strong nonlinear differential equations. The steady state motion and its stability is studied. Results available the discussion of the Sommerfeld effect. A new procedure for determination of parameters of the non-ideal system for which the Sommerfeld effect does not exist is developed. For these critical values of the parameter the Sommerfeld effect is suppressed. In Sect. 3.2, the suggested theoretical consideration is applied for pure nonlinear oscillator driven by a motor with nonlinear torque characteristics. As a special case the pure nonlinear oscillator where the order of the nonlinearity is a positive rational number is investigated. The influence of the order of nonlinearity

L. Cveticanin et al., *Dynamics of Mechanical Systems with Non-Ideal Excitation*,
Mathematical Engineering, DOI 10.1007/978-3-319-54169-3_3

on the dynamic properties of the system is also analyzed. The numerical simulation is done for the motor oscillator system, where the motor torque is a cubic function of the angular velocity and the oscillator is with pure nonlinearity. The obtained results are compared with those obtained analytically (Cveticanin and Zukovic 2015b). In Sect. 3.3, a pure strong nonlinear oscillator which is coupled to a non-ideal source whose torque is a linear function of the angular velocity is considered. An analytical solving procedure based on averaging is developed. The approximate solution has the form of the Ateb function. The resonant case is considered. Steady-state solution and characteristic points are determined. Special attention is given to suppression of the Sommerfeld effect. The section ends with some numerical examples (Cveticanin and Zukovic 2015a). In Sect. 3.4 the non-ideal system with the Duffing oscillator of cubic type is analyzed. The hardening Duffing oscillator with one stable fixed point which is coupled to a non-ideal energy source is mathematically modelled and analytically solved. Approximate solution of the problem is calculated. Condition for the steady-state motion are obtained. Stability of motion is investigated and phenomena of jump in the amplitude-frequency diagram is treated. Using the numerical simulation the chaotic motion is detected. A procedure for controlling chaos is introduced (Zukovic and Cveticanin 2007). Finally, in Sect. 3.5, the non-ideal system with bistable Duffing oscillator, which has three fixed points, is considered. The semi-trivial and non-trivial solutions are determined. Based on the semi-trivial solutions the conditions for quenching of the amplitude of the mechanical system are obtained. In this chapter the stability of non-trivial solutions is investigated. Based on the signs of the Lyapunov exponents (Lyapunov 1893) regions of chaos and hyperchaos are determined (Nbendjo et al. 2012).

3.1 Nonlinear Oscillator Coupled with a Non-ideal Motor with Nonlinear Torque

In the previous chapter the systems which have the following limitations are considered:

- the elastic force of the structure is assumed to be linear (Zukovic and Cveticanin 2009), or with small nonlinearity (Dimentberg et al. 1997; Warminski et al. 2001; Dantas and Balthazar 2006; Felix et al. 2009b),
- the torque property of the motor is assumed to be a linear function of the angular velocity (Dantas and Balthazar 2003; Tsushida et al. 2003 and 2005; Souza et al. 2005a and 2005b; Castao et al. 2010).

In this section a generalization to the model of motor-structure system is done. It is assumed that the elastic property of the system need not be linear or with a small nonlinearity but with a strong nonlinearity of any order, described with any positive rational exponent of the displacement. The motor torque is assumed to be a nonlinear function of angular velocity. No limitation to the form of the forcing torque is introduced. Such a generalization gives us an opportunity to give a more realistic view of the dynamics of the system.

In general, the model of the non-ideal system is an oscillator-motor one which has two degrees of freedom. The motion is described with a system of two coupled differential equations (see Felix et al. 2009b)

$$m\ddot{x} + \hat{f}_1(x) = \hat{f}_2(x, \dot{x}) + \hat{F}(\varphi, \dot{\varphi}, \ddot{\varphi}, \hat{q}), \qquad I\ddot{\varphi} = \mathcal{M}(\dot{\varphi}) + \hat{R}(\varphi, \dot{\varphi}, \ddot{x}, \hat{q}), \quad (3.1)$$

where x and φ are generalized coordinates of the system (displacement and angular position), $\hat{f}_1$ is the deflection function of the oscillator, $\hat{f}_2$ is the function which describes other properties of the oscillator (damping, relaxation, hysteresis...), $\hat{F}$ and $\hat{R}$ are coupling functions of the oscillator and the motor, m is the mass of the oscillator, I is the moment of inertia of the rotating part of the motor and $\hat{q}$ is the measure of the unbalance of the rotor. The deflection function of the oscillator $\hat{f}_1(x)$ is usually assumed to be linear or weakly nonlinear, while the function $\hat{f}_2$ is supposed to be a small one. In general, the torque of the electro-motor is

$$\mathcal{M}(\dot{\varphi}) = L(\dot{\varphi}) - H(\dot{\varphi}), \quad (3.2)$$

where $\dot{\varphi}$ is the angular velocity of the motor and $L(\dot{\varphi})$ and $H(\dot{\varphi})$ are driving and resisting torques. The torque property of the motor is usually assumed to be a linear function of the angular velocity

$$\mathcal{M}(\dot{\varphi}) = V_m^* - C_m^* \dot{\varphi}, \quad (3.3)$$

where C_m^* and V_m^* are characteristics of the motor (Felix et al. 2009b). Comparing the real motor torque with the (3.3) it is evident that the assumed model represents the first approximation of the real one.

The aim is to make the generalization of the problem on non-ideal systems considering the whatever any nonlinear oscillator and the improved version of the motor torque model. The function $\hat{f}_1(x)$ in (3.1) need not to be a small nonlinear function, but may be a strong nonlinear one. The elastic force in the oscillator is the function of any rational order of the displacement (integer or non-integer). Besides, the motor torque (3.2) need not to be a linear velocity function (3.3), but it may be a nonlinear one.

3.1.1 Nonlinear Motor Torque Property

As it is stated by Nayfeh and Mook (1979), for determination of the influence of the motion on the motor properties it is necessary to know the characteristics of the motor. Kononenko and Korablev (1959) plotted experimentally obtained torques as a function of the frequency or angular velocity of rotor for various types of DC motors, for an asynchronous and a synchronous motor. For the most of the mentioned characteristics it is common that they are nonlinear.

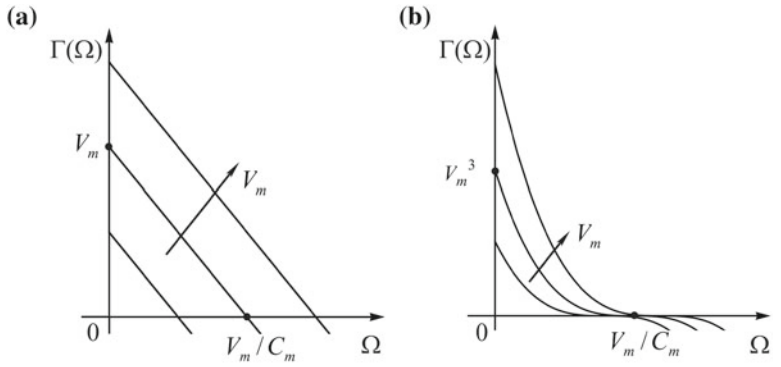

Fig. 3.1 Torque curves for various values of control parameter V_m and constant parameter n: **a** linear property ($n = 1$), **b** cubic property ($n = 3$)

The DC series wound motor, which is considered in this section, has a net of nonlinear characteristics for various constant control or regulator parameters (see Kononenko 1969). Mathematical model of the motor characteristics is assumed in the form

$$\mathcal{M}(\dot{\varphi}) = (V_m^* - C_m^* \dot{\varphi})^n, \tag{3.4}$$

where V_m^* and C_m^* are constant parameters and $n = 2, 3, 4, \ldots$ is a positive integer. It should be mentioned that the relation (3.4) includes the linear model (3.3) for $n = 1$. The DC series wound motor develops a large torque and can be operated at low speed. It is a motor that is well suited for starting heavy loads. Because of that it is often used for industrial cranes and winches, where very heavy loads must be moved slowly and lighter loads moved very rapidly. Introducing the dimensionless time parameter τ, the relation (3.4) transforms into

$$\Gamma(\Omega) = (V_m - C_m \Omega)^n, \tag{3.5}$$

where $\Gamma(\Omega)$ is the dimensionless driving torque with dimensionless parameters V_m and C_m and angular velocity Ω.

In Fig. 3.1 the torque curves for various values of control parameter V_m and constant parameter n are plotted: (a) linear property ($n = 1$), (b) cubic property ($n = 3$). It can be concluded that for increasing of the control parameter V_m the curves move to right in the $\Gamma(\Omega) - \Omega$ plane. For the arbitrary value of the motor frequency, the higher the control parameter V_m, the higher the value of the torque $\Gamma(\Omega)$. In Fig. 3.2, the torque curves for constant value of parameter V_m and various values of the order of nonlinearity is plotted. Increasing the order of nonlinearity n the curves move to the left in the $\Gamma(\Omega) - \Omega$ plane.

Namely, for a certain constant frequency, the motor torque is higher if the order of nonlinearity n is smaller. Nevertheless, the driving torque is zero and independent on the order n for the angular velocity $\Omega = V_m / C_m$. The higher the control parameter

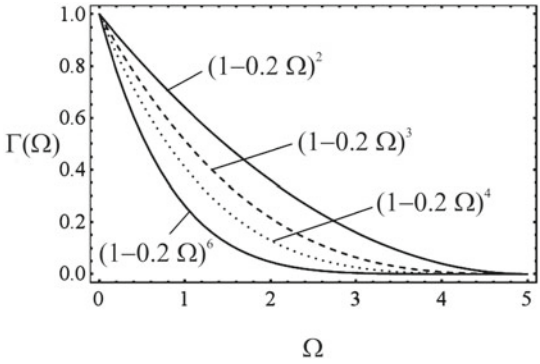

Fig. 3.2 Torque curves for various values of the nonlinearity order n and constant control parameter V_m

V_m, the higher the value of the angular velocity Ω for which the driving torque is zero.

3.1.2 Solution Procedure in General

Introducing the motor characteristics (3.5) into (3.1) and after some modification dimensionless differential equations follow as

$$y'' + f_1(y) = f_2(y, y') + F(\varphi, \varphi', \varphi'', q), \tag{3.6}$$

$$\varphi'' = \Gamma(\varphi') + R(\varphi, \varphi', y'', q), \tag{3.7}$$

where y and φ are the dimensionless generalized coordinates, q is the dimensionless unbalance measure, f_1, f_2, F, R and Γ are the functions of the dimensionless coordinates and parameters and $(') = \mathrm{d}/\mathrm{d}\tau$, $('') = \mathrm{d}^2/\mathrm{d}\tau^2$ with dimensionless time τ.

To classify the 'small' and 'arge' values in the system (3.6), (3.7), we introduce a small parameter $\varepsilon << 1$. Due to the physical sense of the problem the functions f_2, F, R and Γ are small and we have

$$y'' + f_1(y) = \varepsilon f_2(y, y') + \varepsilon F(\varphi, \varphi', \varphi'', q), \tag{3.8}$$

$$\varphi'' = \varepsilon^2 \Gamma(\varphi') + \varepsilon^2 R(\varphi, \varphi', y'', q). \tag{3.9}$$

The terms on the right side of Eqs. (3.8) and (3.9) are small values of the first and second order, respectively, but different from zero. It must be mentioned that, in this paper, we analyze the system with small foundation damping and in the Eq. (3.8) the damping term is of order ε.

In the previous investigation it was assumed that the function $f_1(y)$ is a linear one, and the Eq. (3.8) is with small perturbed terms on the right-hand side of the equation. In this paper the generalization of the problem is done, as the function $f_1(y)$ need not

be linear. The suggested mathematical procedure is based on the method described for the perturbed linear differential equation.

If $\varepsilon = 0$ the Eqs. (3.8) and (3.9) simplify into two uncoupled differential equations

$$y'' + f_1(y) = 0, \qquad \varphi'' = 0. \tag{3.10}$$

For the case when $f_1(y)$ is the linear deflection function, the differential equation (3.10) is a linear one and has the exact solution in the form of the trigonometric function. Otherwise, the trigonometric function represents only the approximate solution of the nonlinear differential equation (3.10). In the papers (Cveticanin 2009; Cveticanin 2009; Cveticanin and Pogany 2012) it is already shown that the approximate solution of trigonometric type is very close to the numerical solution of (3.10) and represents a satisfactory asymptotic solution. It gives as the opportunity to assume the asymptotic solution to (3.10) in the form

$$y = a\cos(\omega(a)t + \psi), \qquad \varphi' = \Omega, \tag{3.11}$$

where a, ψ and Ω are arbitrary constants which satisfy the initial conditions. It is worth to say that the frequency of vibration ω of the nonlinear differential equation (3.10) depends on the amplitude a and has to satisfy exactly or approximately the relation

$$-a\omega^2\cos(\omega t + \psi) + f_1(a\cos(\omega t + \psi)) \approx 0. \tag{3.12}$$

It is of special interest to consider the resonant case (see Cveticanin 1995), when the difference between the frequency of vibration of the structure $\omega(a)$ and of the driving frequency Ω is small. Due to the fact that ω depends on a, there is a trace of frequencies which have to satisfy the relation

$$\Omega - \omega(a) = (\varepsilon\sigma)^2, \tag{3.13}$$

where $\varepsilon\sigma << 1$. The solution of (3.11) and its first time derivative for the resonant case are

$$y = a\cos(\varphi + \psi), \qquad y' = -a\Omega\sin(\varphi + \psi). \tag{3.14}$$

The method suggested in this paper requires the solution of (3.8) and (3.9) to be close to (3.14) which is the solution of (3.11). Namely, the solution of (3.8) is the perturbed version of (3.14), where the parameters are time variable. Using the procedure given by Kononenko (1969) and Cveticanin (1992) the solution of (3.8) is suggested in the form

$$y = a(\tau)\cos(\varphi(\tau) + \psi(\tau)) \equiv a\cos(\varphi + \psi), \tag{3.15}$$

and

$$y' = -a(\tau)\Omega(\tau)\sin(\varphi(\tau) + \psi(\tau)) \equiv -a\Omega\sin(\varphi + \psi). \tag{3.16}$$

The first time derivative of (3.15) is

$$y' = a'\cos(\varphi+\psi) - a(\Omega'+\psi')\sin(\varphi+\psi). \tag{3.17}$$

Comparing (3.17) with (3.16), it follows

$$a'\cos(\varphi+\psi) - a\psi'\sin(\varphi+\psi) = 0. \tag{3.18}$$

Substituting the solution (3.15) and the corresponding first (3.16) and second time derivative of (3.16) into (3.8), we obtain

$$\begin{aligned} &-a'\Omega\sin(\varphi+\psi) - a\Omega(\Omega+\psi')\cos(\varphi+\psi) - a\Omega'\sin(\varphi+\psi) \\ &+f_1(a\cos(\varphi+\psi)) \\ &= \varepsilon f_2(a\cos(\varphi+\psi), -a\omega\sin(\varphi+\psi)) + \varepsilon F(\psi,\Omega,\Omega',q), \end{aligned} \tag{3.19}$$

where according to (3.11) the differential equation (3.9) transforms into two first order differential equations

$$\Omega' = \varepsilon^2\Gamma(\Omega) + \varepsilon^2 R, \tag{3.20}$$

$$\varphi' = \Omega, \tag{3.21}$$

with

$$R = R(\varphi,\Omega,-a\Omega^2\cos(\varphi+\psi),q).$$

Using the relation (3.12) and neglecting terms with the second order small parameter $O(\varepsilon^2)$, the relation (3.18) with (3.19) gives two first order differential equations

$$a' = -\frac{\varepsilon}{\Omega}(F+f_2)\sin(\varphi+\psi) + a(\Omega^2-\omega^2)\sin(\varphi+\psi)\cos(\varphi+\psi) \tag{3.22}$$

$$a\psi' = -a\frac{\Omega^2-\omega^2}{\Omega}\cos^2(\varphi+\psi) - \frac{\varepsilon(F+f_2)}{\Omega}\cos(\varphi+\psi) \tag{3.23}$$

where

$$F = F(\varphi,\Omega,\Omega',q), \qquad f_2 = f_2(a\cos(\varphi+\psi), -a\Omega\sin(\varphi+\psi)).$$

Equations (3.20)–(3.23) are four first order differential equations which correspond to two second order differential equations (3.8) and (3.9). Our task is to solve and analyze these equations.

Averaging procedure

Due to complexity of Eqs. (3.20)–(3.23) it is a heavy task to solve them. This is the reason that the approximate solution procedure for the system of differential equations (3.20)–(3.23) is introduced. In order to eliminate all resonances for the

dynamic system described with (3.22) and (3.23), we define the resonant surface by rewriting the relation (3.13) into

$$\Omega(\tau) - \omega(a) = (\varepsilon\sigma)^2,$$

with $a = a(\tau)$. Now, we perform the averaging over the slow varying variables and apply the standard averaging procedure (see Zhuravlev and Klimov 1988; Cveticanin 1993, 2003). Averaging Eqs. (3.20)–(3.23) over the period of vibration gives

$$a' = -\frac{1}{\Omega}(\bar{F}(\psi, \Omega, q) + \bar{f}_2(a)), \tag{3.24}$$

$$a\psi' = -a\frac{\Omega^2 - \omega^2}{2\Omega} - (\bar{F}^*(\psi, \Omega, q) + \bar{f}_2^*(a)), \tag{3.25}$$

$$\Omega' = \Gamma(\Omega) + \bar{R}(\psi, \Omega, a, q), \tag{3.26}$$

where $\bar{F}$, $\bar{F}^*$, $\bar{f}_2$, $\bar{f}_2^*$ and $\bar{R}$ are averaged functions F, f_2 and R, respectively. Equations (3.24) and (3.25) give variations of the amplitude and initial phase of vibration of the oscillator, while (3.26) describes the variation of the averaged angular velocity of the motor. Solving these equations we obtain $a - t$, $\psi - t$ and $\Omega - t$ relations for various values of parameter. Equations describe the non-stationary motion of the system and give us very objective qualitative analysis of the problem.

It is of special interest to study the influence of the motion of the motor on the oscillator, but also of the oscillator on the motor. It requires the analysis of the coupled system of differential equations (3.24)–(3.26). Solutions $a - t$ and $\Omega - t$ have to be compared with corresponding relations for the case when there is not an interaction between the support and the motor. Then, $\bar{F} = \bar{R} = 0$ and the Eqs. (3.24)–(3.26) simplify into

$$a' = -\frac{\bar{f}_2(a)}{\omega(a)}, \qquad \xi' = \frac{\bar{f}_2^*(a)}{a}, \tag{3.27}$$

$$\Omega' = \Gamma(\Omega). \tag{3.28}$$

Separating variables in Eqs. $(3.27)_1$ and (3.28) and after some calculation, we have

$$s(a_0) - s(a) = \tau, \tag{3.29}$$

$$\Gamma_1(\Omega) - \Gamma_1(\Omega_0) = \tau, \tag{3.30}$$

where

$$s(a) = \int \frac{\bar{f}_2(a)}{\omega(a)} da, \qquad \Gamma_1(\Omega) = \int \frac{d\Omega}{\Gamma(\Omega)},$$

a_0 is the initial amplitude of the oscillator vibration and Ω_0 is the initial angular velocity of the motor. Based on $(3.27)_2$ and (3.29) the $\psi - a$ and $\psi - \tau$ relations, for the initial phase of vibration of the oscillator, are calculated.

Comparing Eqs. (3.24)–(3.26) and (3.27), (3.28), it is evident that the most significant difference in amplitude and angular velocity is for the resonant case when the difference between the angular velocity of the motor Ω and the eigenfrequency of the oscillator ω is quite small.

3.1.3 Steady-State Motion and Its Stability

The steady state motion of the coupled oscillator-motor system is described with the system of three algebraic equations

$$\bar{F}(\psi, \Omega, q) + \bar{f}_2(a) = 0, \tag{3.31}$$

$$a\frac{\Omega^2 - \omega^2}{2\Omega} + \bar{F}^*(\psi, \Omega, q) + \bar{f}_2^*(a) = 0, \tag{3.32}$$

$$\Gamma(\Omega) + \bar{R}(\psi, \Omega, a, q) = 0, \tag{3.33}$$

which represent right-hand sides of Eqs. (3.24)–(3.26). Eliminating the parameter ξ by combining Eqs. (3.31) and (3.32), and also (3.31) and (3.33), a system of two algebraic equations is obtained

$$Q_1(a, \Omega, q) = 0, \qquad Q_2(a, \Omega, q, V_m) = 0, \tag{3.34}$$

where equations give $a - \Omega$ relations for various values of q and parameter V_m of the driving torque (see Eq. (3.3)). Algebraic equations (3.34) are nonlinear and very complex. The solution of (3.34) gives the amplitude of oscillator vibration and the angular velocity of motor for the steady state motion. Very often, the solution of (3.34) is analyzed graphically by plotting of the frequency-response curves $a - \Omega$ for the oscillator (relation $(3.34)_1$) and the motor (relation $(3.34)_2$). The intersection of the curves give us the steady-state parameters of the system.

To analyze the stability of the steady-state solution the Jacobi determinant is formed

$$J = \begin{bmatrix} \frac{d\bar{f}_2(a)}{da} & \frac{\partial \bar{F}}{\partial \psi} & \frac{\partial \bar{F}}{\partial \Omega} \\ \frac{\Omega^2 - \omega^2}{2\Omega} - \frac{a\omega}{\Omega}\frac{d\omega}{da} + \frac{\bar{f}_2^*(a)}{da} & \frac{\partial \bar{F}^*}{\partial \psi} & \frac{\partial \bar{F}^*}{\partial \Omega} - a \\ \frac{\partial \bar{R}}{\partial a} & \frac{\partial \bar{R}}{\partial \psi} & \frac{\partial \bar{R}}{\partial \Omega} + \frac{d\Gamma}{d\Omega} \end{bmatrix}. \tag{3.35}$$

The characteristic equation is

$$J_3\lambda^3 + J_2\lambda^2 + J_1\lambda + J_0 = 0, \tag{3.36}$$

where

$$J_3 = 1, \qquad J_2 = -\left(\frac{d\bar{f}_2(a)}{da} + \frac{\partial \bar{F}^*}{\partial \psi} + \frac{\partial \bar{R}}{\partial \Omega} + \frac{d\Gamma}{d\Omega}\right), \qquad J_0 = -\det(J),$$
$$J_1 = \left(\frac{d\bar{f}_2(a)}{da} + \frac{\partial \bar{F}^*}{\partial \psi}\right)\left(\frac{\partial \bar{R}}{\partial \Omega} + \frac{d\Gamma}{d\Omega}\right) + \frac{d\bar{f}_2(a)}{da}\frac{\partial \bar{F}^*}{\partial \psi}$$
$$+\frac{\partial \bar{F}}{\partial \psi}\left(\frac{\Omega^2 - \omega^2}{2\Omega} - \frac{a\omega}{\Omega}\frac{d\omega}{da} + \frac{\bar{f}_2^*(a)}{da}\right)$$
$$-\frac{\partial \bar{F}}{\partial \Omega}\frac{\partial \bar{R}}{\partial a} - \frac{\partial \bar{R}}{\partial \psi}\left(\frac{\partial \bar{F}^*}{\partial \Omega} - a\right). \tag{3.37}$$

Using the Routh–Hurwitz criteria it can be concluded that the stability for the steady-state solution (3.31)–(3.33) is satisfied if

$$J_0 > 0, \qquad J_1 > 0, \qquad J_2 > 0, \qquad J_1 J_2 - J_0 J_3 > 0. \tag{3.38}$$

3.1.4 Characteristic Points on the Steady State Curves

Let us determine the locus of characteristic points and characteristic control parameter in the frequency-response curve $(3.34)_1$ where the jump phenomena appears (see Fig. 3.3). The criteria is that at these points P and R the both curves given with (3.34) have the same direction of the joint tangent. Namely, for

$$dQ_1 = \frac{\partial Q_1}{\partial \Omega}d\Omega + \frac{\partial Q_1}{\partial a}da = 0, \qquad dQ_2 = \frac{\partial Q_2}{\partial \Omega}d\Omega + \frac{\partial Q_2}{\partial a}da = 0, \tag{3.39}$$

the equality of the direction of the tangents of the curves $(3.34)_1$ and $(3.34)_2$ in P is

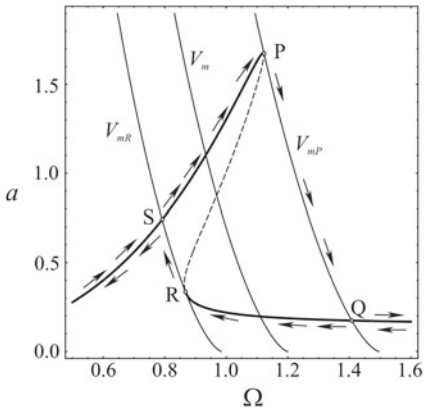

Fig. 3.3 Characteristic points

$$\frac{da}{d\Omega} \equiv -\left(\frac{\frac{\partial Q_1}{\partial \Omega}}{\frac{\partial Q_1}{\partial a}}\right)_{\Omega_P, a_P, V_{mP}} = -\left(\frac{\frac{\partial Q_2}{\partial \Omega}}{\frac{\partial Q_2}{\partial a}}\right)_{\Omega_P, a_p, V_{mp}}. \tag{3.40}$$

Solving algebraic equations (3.40) and also (3.34), values Ω_P, a_P, V_{mP} for a peak point are obtained. The frequency Ω_P corresponds to the amplitude a_P and gives the control parameter for motor torque V_{mP}. Using the value of the control parameter V_{mP}, Eq. (3.34) give us the additional pair of (Ω_Q, a_Q) values due to the fact that system of algebraic equations is nonlinear. Points P and Q correspond to the same value of control parameter V_{mP}.

The same procedure is applied for determining the Ω_R, a_R, V_{mR} and also (Ω_S, a_S) which corresponds to V_{mR}. The critical frequency Ω_R with correspondent amplitude a_R gives the value of the control parameter V_{mR} for which the jump phenomena to the point S appears during decreasing of the control parameter V_m. In the region between V_{mP} and V_{mR} in the amplitude-frequency diagram a gap exists.

To eliminate the Sommerfeld effect the control parameter V_m has to be beyond the interval (V_{mP}, V_{mR}). The number of stable steady-state solutions outside this interval is only one.

3.1.5 *Suppression of the Sommerfeld Effect*

The Sommerfeld effect does not appear if, for all of values of the driving torque, only one steady-state response of the oscillator exists. Then, the intersection between the amplitude-frequency curves of the oscillator and of the motor has only one unique solution. Using this criteria the parameters of the system have to be calculated. For technical reasons we suggest an approximate analytical method for determination of the parameters of the non-ideal system where Sommerfeld effect does not exist. The basic requirement of the method is that the bone curve $Q_3(a, \Omega)$ of the amplitude-frequency characteristic of the oscillator $(3.34)_1$ and the amplitude-frequency curve of the motor $(3.34)_2$ have the equal gradient for the extreme steady-state position (a^*, Ω^*). Namely, the following relations have to be satisfied

$$Q_1(a^*, \Omega^*, q^*) = 0, \quad Q_2(a^*, \Omega^*, q^*, V_m^*) = 0, \quad Q_3(a^*, \Omega^*) = 0,$$
$$\frac{da}{d\Omega} \equiv -\left(\frac{\frac{\partial Q_1}{\partial \Omega}}{\frac{\partial Q_1}{\partial a}}\right)_{\Omega^*, a^*, V_m^*, q^*} = -\left(\frac{\frac{\partial Q_3}{\partial \Omega}}{\frac{\partial Q_3}{\partial a}}\right)_{\Omega^*, a^*, V_m^*, q^*}. \tag{3.41}$$

Solving the system of algebraic equations (3.41) the parameter q^* is obtained, for which only one solution for Ω^*, a^* and V_m^* exists. Due to the fact that for either value of the control parameter V_m the amplitude-frequency curve $(3.34)_2$ remains parallel to $Q_2(a, \Omega, q^*, V_m^*) = 0$ and also to the bone curve $Q_3(a, \Omega) = 0$ it can be concluded that there is only one intersection between any $Q_2(a, \Omega, q^*, V_m) = 0$ and the amplitude-frequency curve $Q_1(a, \Omega, q^*) = 0$.

Remark 1 Using the same relations (3.41) instead of q^* another critical parameter of the system can be calculated (for example C_m^*).

3.1.6 Conclusion

Analyzing the results the following is concluded:

1. The generalized non-ideal mechanical system contains the nonlinear oscillator of any order and a motor with the driving torque which need not to be the linear function of the angular velocity.
2. The approximate solution procedure of the problem suggested in the text is suitable for the near resonant case and gives the results which are possible to be used for the stability analysis and discussion of the characteristic properties of the system.
3. The approximate value of the control parameter for the non-ideal source is analytically calculated applying the method of equating the gradient of the both amplitude-frequency curves (of the oscillator and of the motor) in the intersection points. The criteria for the Sommerfeld effect is obtained.
4. It can be concluded that the method developed in the text gives the parameter values for which the Sommerfeld effect is suppressed. For these parameters there exists only one steady-state response of the oscillator for all values of the driving torque.
5. The suitable choice of non-ideal system parameters available the motion without jumps.
6. The analytically obtained results show a good agreement with numerically obtained ones. It proves the correctness of the analytic procedures.

3.2 Pure Nonlinear Oscillator and the Motor with Nonlinear Torque

Let us consider a motor-structure system shown in Fig. 3.4.

A motor with an unbalance is connected to a viscoelastic structure with nonlinear properties. The motion occurs in a horizontal plane and is constrained so that the motor executes a rectilinear motion along the x -axis. The elastic force of the structure is assumed as a pure nonlinear displacement function

$$F_e = kx\,|x|^{\alpha-1}\,, \tag{3.42}$$

where $\alpha \geq 1$ and $\alpha \in \mathbb{R}$ is a positive rational number (integer or non-integer) which represents the order of nonlinearity and k is the coefficient of rigidity. Experimental investigation on a significant number of materials, for example: aluminum, titanium

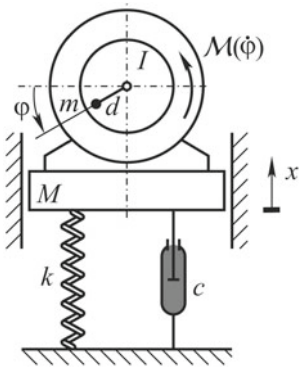

Fig. 3.4 Model of the motor-structure non-ideal system

and other aircraft materials (Prathap and Varadan 1976), copper and copper alloys (Lo and Gupta 1978), aluminum alloys and annealed copper (Lewis and Monasa 1982), wood (Haslach 1985), ceramic materials (Colm and Clark 1988), hydrophilic polymers (Haslach 1992; Pilipchuk 2010), composites (Chen and Gibson 1998), polyurethane foam (Patten et al. 1998), felt (Russell and Rossing 1998), etc., show that the stress-strain properties of the material are nonlinear. The nonlinear dependence of the restoring force on the deflection is a polynomial whose exponent is of positive integer or non-integer order. For most of these materials the damping properties are also nonlinear. However, for the mentioned metallic materials and their alloys the order of nonlinearity in the damping force is small and the linear damping force model gives a good approximation. Thus, the damping force-velocity function is

$$F_d = c\dot{x}, \tag{3.43}$$

where c is the damping constant. Mass of the system is M, the moment of inertia of the motor rotor is J, mass of the rotor unbalance is m and the length of the rotor unbalance is d. The considered non-ideal system has two degrees-of-freedom, represented by the generalized coordinates x and φ and the motion is described with two Lagrange differential equations

$$\begin{aligned} \frac{d}{dt}\frac{\partial T}{\partial \dot{x}} - \frac{\partial T}{\partial x} + \frac{\partial U}{\partial x} + \frac{\partial \Phi}{\partial \dot{x}} &= Q_x, \\ \frac{d}{dt}\frac{\partial T}{\partial \dot{\varphi}} - \frac{\partial T}{\partial \varphi} + \frac{\partial U}{\partial \varphi} + \frac{\partial \Phi}{\partial \dot{\varphi}} &= Q_\varphi, \end{aligned} \tag{3.44}$$

where T is the kinetic energy, U is the potential energy, Φ is the dissipative function and Q_x and Q_φ are the generalized forces. The kinetic energy, potential energy and the dissipation function are expressed by

$$T = \frac{1}{2}M\dot{x}^2 + \frac{1}{2}m(\dot{x} - d\dot{\varphi}\cos\varphi)^2 + \frac{1}{2}m(d\dot{\varphi}\sin\varphi)^2 + \frac{1}{2}J\dot{\varphi}^2, \tag{3.45}$$

$$U = \frac{k}{\alpha+1}x^{\alpha+1}, \qquad \Phi = \frac{1}{2}c\dot{x}^2, \tag{3.46}$$

where $\varepsilon << 1$ and a dot denotes differentiation with respect to time t. For the driving torque (3.2) the generalized forces are

$$Q_x = 0, \qquad Q_\varphi = \mathcal{M}(\dot{\varphi}). \tag{3.47}$$

Equations of motion (3.44) have the form

$$\begin{aligned} \ddot{x}(M+m) + kx\,|x|^{\alpha-1} + c\dot{x} - md(\ddot{\varphi}\cos\varphi - \dot{\varphi}^2\sin\varphi) = 0, \\ (J+md^2)\ddot{\varphi} - md\ddot{x}\cos\varphi = \mathcal{M}(\dot{\varphi}), \end{aligned} \tag{3.48}$$

and the initial conditions are

$$x(0) = x_0,\ \dot{x}(0) = 0,\ \varphi(0) = 0,\ \dot{\varphi}(0) = \omega_0. \tag{3.49}$$

It is convenient to normalize the coordinates and time according to

$$x \longrightarrow y = x/l, \qquad t \longrightarrow \tau = \Omega^* t, \tag{3.50}$$

where l is the initial length of the non-deformed spring and Ω^* is the synchronous angular velocity of the rotor. By introducing (3.50) the differential equations (3.48) transform into

$$\begin{aligned} y'' + \varepsilon\zeta_1 y' + p^2 y\,|y|^{\alpha-1} = \varepsilon\mu_1(\varphi''\cos\varphi - \varphi'^2\sin\varphi), \\ \varphi'' = \varepsilon^2[\eta_2 y''\cos\varphi + \mathcal{M}(\varphi')], \end{aligned} \tag{3.51}$$

with non-dimensional initial conditions

$$y(0) = A,\ y'(0) = 0,\ \varphi(0) = 0,\ \varphi'(0) = \frac{\omega_0}{\Omega^*} = \omega, \tag{3.52}$$

where

$$\begin{aligned} p = \frac{\omega^*}{\Omega^*}, \qquad \omega^{*2} = \frac{kl^{\alpha-1}}{M+m}, \qquad A = \frac{x_0}{l}, \qquad \varepsilon = \frac{m}{M+m}, \\ \varepsilon\mu_1 = \left(\frac{m}{M+m}\right)\left(\frac{d}{l}\right), \qquad \varepsilon^2\eta_2 = \left(\frac{d}{l}\right)\frac{ml^2}{(J+md^2)}, \\ \varepsilon\zeta = \left(\frac{m}{M+m}\right)\frac{c}{\Omega^* m}, \qquad \varepsilon^2\mathcal{M}(\varphi') = \frac{\mathcal{M}(\Omega^*\varphi')}{(J+md^2)\Omega^{*2}}, \end{aligned} \tag{3.53}$$

Ω^* is the synchronous angular velocity (Dimentberg et al. 1997) and prime denotes differentiation with respect to τ. It is worth to say that $\varepsilon << 1$ is a small positive parameter. Using the expression (3.51) we have

$$y'' + p^2 y\,|y|^{\alpha-1} = -\varepsilon(\mu_1 \varphi'^2 \sin\varphi + \zeta_1 y'), \tag{3.54}$$

$$\varphi'' = \varepsilon^2[\mathcal{M}(\varphi') - \eta_2 p^2 y\,|y|^{\alpha-1}\cos\varphi]. \tag{3.55}$$

The Eqs. (3.54) and (3.55) represent the system of two coupled differential equations which describe the motion of the non-ideal system given in Fig. 3.4. Comparing (3.54) and (3.55) with (3.8) and (3.9) we have

$$f_1 = p^2 y\,|y|^{\alpha-1}, \quad f_2 = -\zeta_1 y', \quad F = -\mu_1 \varphi'^2 \sin\varphi, \quad R = -\eta_2 p^2 y\,|y|^{\alpha-1}\cos\varphi. \tag{3.56}$$

Now, the differential equations (3.54) and (3.55) have to be solved.

3.2.1 Approximate Solution Procedure

For the case when the small parameter ε tends to zero, the differential equations (3.54) and (3.55) transform into

$$y'' + p^2 y\,|y|^{\alpha-1} = 0, \qquad \varphi'' = 0. \tag{3.57}$$

The two differential equations (3.57) are uncoupled and can be solved independently but according to the initial conditions (3.52). Equation $(3.57)_1$ is a second order pure nonlinear differential equation with rational order of nonlinearity. The approximate analytical solution of the $(3.57)_1$ is assumed in the form of a harmonic function $(3.11)_1$ with the frequency (see Cveticanin 2009; Cveticanin and Pogany 2012)

$$\omega = \omega_\alpha \sqrt{p^2} a^{(\alpha-1)/2}, \tag{3.58}$$

where

$$\omega_\alpha = \sqrt{\frac{\alpha+1}{2}} \frac{\sqrt{\pi}\,\Gamma\left(\frac{3+\alpha}{2(\alpha+1)}\right)}{\Gamma\left(\frac{1}{\alpha+1}\right)}, \tag{3.59}$$

and Γ is the gamma function (Gradstein and Rjizhik 1971). The relation (3.58) is the exact analytically obtained frequency of vibration of the nonlinear elastic structure $(3.57)_1$. The asymptotic solution $(3.11)_1$ approximately satisfies the differential equation $(3.57)_1$, i.e.,

$$-a\omega^2 \cos(\omega t + \psi) + p^2 a^\alpha \cos^\alpha(\omega t + \psi) \approx 0. \tag{3.60}$$

Using the generalized procedure given in Sect. 3.3 and substituting the approximate solution with time variable parameters (3.15) and the corresponding derivatives into (3.54) it follows

$$\begin{aligned} &-a'\Omega\sin(\varphi+\psi)-a\Omega(\Omega+\psi')\cos(\varphi+\psi) \\ &+p^2a^\alpha\cos^\alpha(\varphi+\psi) \\ &=-\varepsilon\mu_1\Omega^2\sin\varphi+\varepsilon\zeta_1 a\Omega\sin(\varphi+\psi), \end{aligned} \tag{3.61}$$

where for the resonant condition (3.13) and using the relation (3.60), the differential equation (3.61) simplifies into

$$-a'\Omega\sin(\varphi+\psi)-a(\Omega^2-\omega^2+\Omega\varphi')\cos(\varphi+\psi)=\varepsilon\mu_1\Omega^2\sin\phi+\varepsilon\zeta_1 a\Omega\sin(\varphi+\psi). \tag{3.62}$$

The relations (3.18) and (3.62) are the two first order differential equations which correspond to the second order differential equation (3.54). Solving the Eqs. (3.18) and (3.62) for a' and ψ' the relations (3.22) and (3.23) for (3.116) follow

$$\begin{aligned} a' &= \varepsilon\mu_1\Omega\sin\varphi\sin(\varphi+\psi)-\varepsilon\zeta_1 a\sin^2(\varphi+\psi) \\ &\quad -a\frac{\Omega^2-\omega^2}{\Omega}\sin(\varphi+\psi)\cos(\varphi+\psi), \end{aligned} \tag{3.63}$$

$$\begin{aligned} a\psi' &= -a\frac{\Omega^2-\omega^2}{\Omega}\cos^2(\varphi+\psi)-\varepsilon\mu_1\Omega\sin\varphi\cos(\varphi+\psi) \\ &\quad +\varepsilon\zeta_1 a\sin(\varphi+\psi)\cos(\varphi+\psi). \end{aligned} \tag{3.64}$$

Substituting the solution (3.15) into the differential equation (3.55) and using the relations (3.56) and (3.60) we obtain (3.20) with (3.21), i.e.,

$$\Omega'=\varepsilon^2\mathcal{M}(\Omega)-\varepsilon^2\eta_2 a\omega^2\cos(\varphi+\psi)\cos\varphi, \qquad \varphi'=\Omega. \tag{3.65}$$

Equations (3.63)–(3.65) represent the four first order differential equations which correspond to the second order differential equations (3.54) and (3.55). After averaging equations transform into

$$a'=-\frac{\zeta_1 a}{2}+\frac{\mu_1\Omega}{2}\cos\psi, \tag{3.66}$$

$$\psi'=-\frac{\Omega^2-\omega^2}{\Omega}+\frac{\mu_1\Omega}{2a}\sin\psi, \tag{3.67}$$

$$\Omega'=\mathcal{M}(\Omega)-\frac{\eta_2 a\Omega^2}{2}\cos\psi. \tag{3.68}$$

Equations (3.66)–(3.68) describe the non-stationary motion of the system.

3.2.2 Steady-State Motion and Its Properties

If there is no interaction between the oscillator and the motor the amplitude of vibration of the oscillator decreases exponentially from the initial amplitude A (due

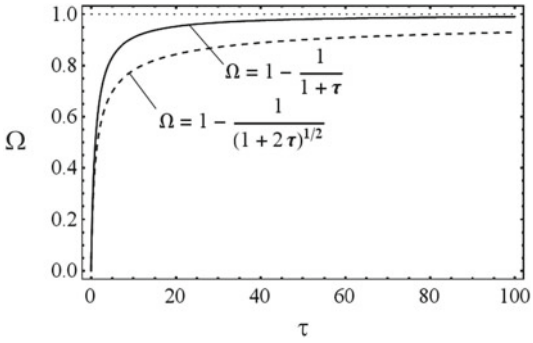

Fig. 3.5 $\Omega - \tau$ curves for various values of the nonlinearity order n: $n = 2$ (*full line*), $n = 3$ (*dotted line*)

to viscous damping) as $a = A\exp(-\gamma\tau/2)$, and the variation of the angular velocity of the motor satisfies the relation

$$\Omega = \frac{V_m}{C_m} - \frac{V_m}{C_m}\frac{1}{(1 + C_m V_m^{n-1}(n-1)\tau)^{1/(n-1)}}. \tag{3.69}$$

In Fig. 3.5, $\Omega - \tau$ curves for various values of parameter n are plotted.

Namely, for $V_m = 1$ and $C_m = 1$ the $\Omega - \tau$ relations according to (3.69) are: for $n = 2$

$$\Omega = 1 - \frac{1}{1+\tau}, \tag{3.70}$$

for $n = 3$

$$\Omega = 1 - \frac{1}{(1+2\tau)^{1/2}}. \tag{3.71}$$

Analyzing the relations (3.69) i.e., (3.70) and (3.71), it is obvious that for any value of parameter n, the angular velocity is zero for $\tau = 0$, and tends to the constant steady-state value V_m/C_m. The smaller the value of the parameter n, the steady-state value is achieved in a shorter time.

For the steady-state respons, Eqs. (3.66)–(3.68) have the form

$$\frac{\zeta_1 a}{2} = \frac{\mu_1\Omega}{2}\cos\psi, \tag{3.72}$$

$$\frac{\Omega^2 - \omega^2}{\Omega}a = \frac{\mu_1\Omega}{2}\sin\psi, \tag{3.73}$$

$$\mathcal{M}(\Omega) = \frac{\eta_2 a\Omega^2}{2}\cos\psi. \tag{3.74}$$

Solving the algebraic equations (3.72)–(3.74), the steady-state properties of the system are determined.

Eliminating ξ from (3.72) and (3.73) and also from (3.72) and (3.74) following two $a - \Omega$ relations are obtained

$$(\mu_1\Omega)^2 = a^2\left(\zeta_1^2 + 4\left(\frac{\Omega^2-\omega^2}{\Omega}\right)^2\right), \tag{3.75}$$

$$\zeta_1 a^2\Omega = 2\frac{\mu_1}{\eta_2}\mathcal{M}(\Omega), \tag{3.76}$$

i.e., after substituting (3.58) and (3.4) it follows

$$(\mu_1\Omega)^2 = a^2\left(\zeta_1^2 + 4\left(\frac{\Omega^2-\omega_\alpha^2 p^2 a^{(\alpha-1)}}{\Omega}\right)^2\right), \tag{3.77}$$

$$\zeta_1 a^2\Omega = 2\frac{\mu_1}{\eta_2}(V_m - C_m\Omega)^n. \tag{3.78}$$

The solution of the system of algebraic equations (3.75) and (3.76) depends on the motor torque function but also on the order of nonlinearity of the oscillator. Solving algebraic equations (3.77) and (3.78) for a and Ω, the steady-state phase angle ψ is calculated. Namely, the relation for phase is

$$2\frac{\Omega^2-\omega^2}{\Omega\zeta_1} = \tan\psi, \tag{3.79}$$

and is obtained by dividing Eqs. (3.72) and (3.73).

3.2.3 Characteristic Points

According to the procedure given in Sect. 3.3, characteristic points in amplitude-frequency curves can be calculated. Solving the system of algebraic equations (3.77) and (3.78) and also the relation

$$\begin{aligned}\frac{da}{d\Omega} &\equiv \frac{2\mu_1^2\Omega^3 - \Omega a^2\zeta_1^2 - 8a^2\left(\Omega^2-\omega^2\right)\Omega}{a\zeta_1^2\Omega^2 + 4a\left(\Omega^2-\omega^2\right)^2 - 4(\alpha-1)a\left(\Omega^2-\omega^2\right)\omega^2} \\ &= -\frac{\zeta_1 a^2 + 2nC_m\frac{\mu_1}{\eta_2}(V_m - C_m\Omega)^{n-1}}{2\zeta_1 a\Omega},\end{aligned}$$

where ω is given as (3.58), the parameters a_P, Ω_P and V_{mP} of the characteristic point P are obtained.

Due to complexity to the suggested calculation an approximate solution procedure is recommended. Using the fact that the locus of the point P is near the position of the point P', where solutions of the Eq. (3.77) bifurcate from one to two, i.e., from three to two real solutions, it is suggested to consider the characteristics of P' instead of P. Thus, for

$$\Omega_{P'} = \omega_{p'} = \omega_\alpha a_{p'}^{(\alpha-1)/2}\sqrt{p^2}, \tag{3.80}$$

the relation (3.77) gives the peak amplitude

$$a_{P'} = \left(\frac{\zeta_1}{\omega_\alpha \mu_1 \sqrt{p^2}}\right)^{\frac{2}{\alpha-3}}. \tag{3.81}$$

Substituting (3.81) into (3.80), the locus $\Omega_{P'}$ for $a_{P'}$ is obtained

$$\Omega_{P'} = \left(\frac{\zeta_1}{\mu_1}\right)^{\frac{\alpha-1}{\alpha-3}} \left(\omega_\alpha \sqrt{p^2}\right)^{\frac{2}{3-\alpha}}. \tag{3.82}$$

Equations (3.81) and (3.82) with (3.78) give the value of a control parameter $V_{mP'}$ of the motor torque

$$V_{mP'} = C_m \left(\frac{\zeta_1}{\mu_1}\right)^{\frac{\alpha-1}{\alpha-3}} \left(\omega_\alpha \sqrt{p^2}\right)^{\frac{2}{3-\alpha}} + \left(\frac{\eta_2}{2}\right)^{\frac{1}{n}} \left(\frac{\zeta_1}{\mu_1}\right)^{\frac{2\alpha}{n(\alpha-3)}} \left(\omega_\alpha \sqrt{p^2}\right)^{\frac{6}{n(3-\alpha)}}. \tag{3.83}$$

For this approximate value of the control parameter $V_{mP'}$ the Sommerfeld effect has to appear. Analyzing the relation (3.77) it is obvious that the position of the extreme point P' is on a line

$$a = \frac{\mu_1}{\zeta_1}\Omega.$$

The gradient of the line does not depend on the order of nonlinearity α, but only on the parameters μ_1 and ζ_1.

3.2.4 *Suppression of the Sommerfeld Effect*

As it is previously shown Eqs. (3.81)–(3.83) give us values $\Omega_{P'}$ and $a_{P'}$ of the point P' and also the corresponding control parameter $V_{mP'}$, which forces the amplitude-frequency torque curve through the point P'. If the amplitude-frequency torque curve and the backbone curve (3.80) have the equal gradients in the P' i.e.,

$$\frac{da}{d\Omega} \equiv \frac{2}{\omega_\alpha(\alpha-1)\sqrt{p^2}a^{\frac{\alpha-3}{2}}} = -\frac{\zeta_1 a^2 + 2nC_m\frac{\mu_1}{\eta_2}(V_m - C_m\Omega)^{n-1}}{2\zeta_1 a\Omega}, \tag{3.84}$$

the additional condition for suppression of the Sommerfeld effect in the system is obtained. Namely, solving the system of four algebraic equations (3.81)–(3.83) and (3.84) four unknown values are obtained: a^*, Ω^*, V_m^* and also α^*, ζ_1^*, μ_1^*, η_2^* or C_m^*. The forth mentioned parameter is the control parameter for elimination of the Sommerfeld effect.

The left side of the Eq. (3.84) is the gradient of the backbone curve in the point P'. Using (3.81) the gradient is

$$\left(\frac{da}{d\Omega}\right)_{P'} = \frac{2\mu_1}{\zeta_1(\alpha-1)}.$$

It depends on the order of nonlinearity α: for $\alpha < 1$ it is negative, for $\alpha > 1$ it is positive, while for $\alpha = 1$ it represents an orthogonal direction. The bending is higher for α significantly higher or smaller than 1.

Using relations (3.81)–(3.83), Eq. (3.84) is rewritten as

$$\frac{4\zeta_1}{1-\alpha} = \gamma + C_m n \mu_1 \left(\frac{2}{\eta_2}\right)^{\frac{1}{n}} \left(\frac{\zeta_1}{\mu_1}\right)^{\frac{2}{n}\left((n-1)+\frac{n-3}{\alpha-3}\right)} \left(\omega_\alpha \sqrt{p^2}\right)^{\frac{2(n-3)}{(3-\alpha)n}}. \tag{3.85}$$

If the order of nonlinearity α and parameters n, γ, μ_1 and η_2 are known, solving the relation (3.85), for example, for the parameter C_m^*, we have

$$C_m^* = \frac{3+\alpha}{1-\alpha}\frac{1}{n}\left(\frac{\eta_2}{2}\right)^{\frac{1}{n}} \left(\frac{\zeta_1}{\mu_1}\right)^{1-\frac{2}{n}\left((n-1)+\frac{n-3}{\alpha-3}\right)} \left(\omega_\alpha \sqrt{p^2}\right)^{\frac{2(n-3)}{(3-\alpha)n}}. \tag{3.86}$$

Substituting (3.86) into (3.87) the control parameter V_m^* is

$$V_m^* = \left(\frac{3+\alpha}{1-\alpha}\frac{1}{n}+1\right)\left(\frac{\eta_2}{2}\right)^{\frac{1}{n}} \left(\frac{\zeta_1}{\mu_1}\right)^{\frac{2\alpha}{n(\alpha-3)}} \left(\omega_\alpha \sqrt{p^2}\right)^{\frac{6}{(3-\alpha)n}}. \tag{3.87}$$

It can be concluded that for parameter values (3.86) and (3.87) in the non-ideal system with known order of nonlinearity α the jump phenomena is excluded.

3.2.5 *Numerical Examples*

In this section, numerical examples of electro-motors connected with pure nonlinear elastic structures are considered. As is shown in the previous section, there are numerous materials whose elastic properties are strong nonlinear. We choose two of them: the copper alloy with $\alpha = 4/3$ and aluminium alloy with $\alpha = 5/3$ (Jutte 2008). The corresponding elastic forces are

$$F_{e1} = kx\,|x|^{1/3}, \qquad F_{e2} = kx\,|x|^{2/3}. \tag{3.88}$$

If the motor-structure system is driven with the motor torque of cubic type

$$\mathcal{M}(\dot{\varphi}) = (V_m^* - C_m^*\dot{\varphi})^3. \tag{3.89}$$

differential equations of motion are:
for $\alpha = 4/3$

$$y'' + p^2 y\,|y|^{1/3} = -\varepsilon(\mu_1 \varphi'^2 \sin\varphi + \zeta_1 y'), \tag{3.90}$$
$$\varphi'' = \varepsilon^2[(V_m - C_m\varphi')^3 - \eta_2 p^2 y\,|y|^{1/3}\cos\varphi], \tag{3.91}$$

for $\alpha = 5/3$

$$y'' + p^2 y\,|y|^{2/3} = -\varepsilon(\mu_1 \varphi'^2 \sin\varphi + \zeta_1 y'), \tag{3.92}$$
$$\varphi'' = \varepsilon^2[(V_m - C_m\varphi')^3 - \eta_2 p^2 y\,|y|^{2/3}\cos\varphi]. \tag{3.93}$$

Corresponding averaged differential equations of motion obtained analytically are

$$a' = -\frac{\zeta_1 a}{2} + \frac{\mu_1 \Omega}{2}\cos\psi, \tag{3.94}$$
$$\xi' = -\frac{\Omega^2 - \omega_\alpha^2 p^2 a^{(\alpha-1)}}{\Omega} + \frac{\mu_1\Omega}{2a}\sin\psi, \tag{3.95}$$
$$\Omega' = (V_m - C_m\Omega)^3 - \frac{\eta_2 a\Omega^2}{2}\cos\psi, \tag{3.96}$$

where dependently on the order α the frequency constants are $\omega_{4/3} = 0.96916$ and $\omega_{5/3} = 0.940\,81$ (see Cveticanin 2009). For $\mu_1 = 0.15$, $\eta_2 = 0.05$, $p^2 = 1$, $C_m = 1$ and $\zeta_1 = 0.1$ the steady-state amplitude-frequency relations (3.77) for these systems are:
for $\alpha = 4/3$

$$0.0225\Omega^2 = a^2\left(0.01 + 4\left(\frac{\Omega^2 - 0.93927a^{1/3}}{\Omega}\right)^2\right), \tag{3.97}$$

for $\alpha = 5/3$

$$0.0225\Omega^2 = a^2\left(0.01 + 4\left(\frac{\Omega^2 - 0.885\,12a^{2/3}}{\Omega}\right)^2\right), \tag{3.98}$$

while the relation (3.78) for the motor is

$$0.1a^2\Omega = 6(V_m - \Omega)^3. \tag{3.99}$$

In Fig. 3.6, amplitude-frequency steady-state diagrams for various values of control parameter V_m and order of nonlinearity α are plotted.

Analytically obtained (full line) curves (3.97)–(3.99) are compared with numerically (3.90)–(3.93) ones, obtained by increasing (circle) and decreasing (squares) of the control parameter V_m. Numerical solutions are obtained applying the Runge–Kutta

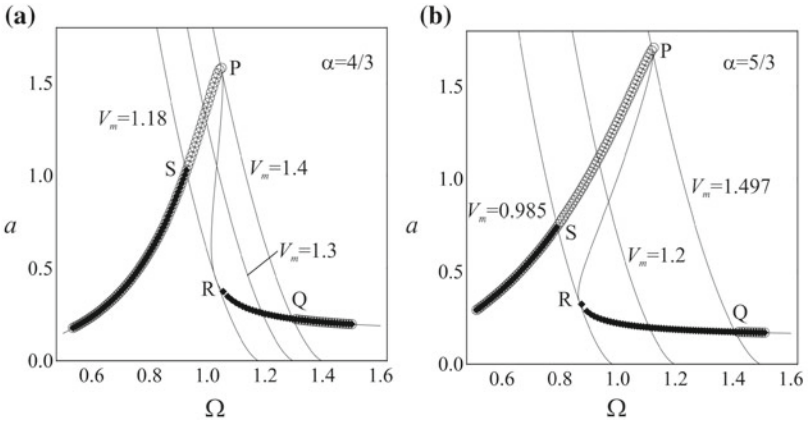

Fig. 3.6 Frequency-response curves for various α obtained: **a** analytically (*full line*), **b** numerically (*circles* - for the increasing of the V_m, *squares* - for decreasing of the V_m)

Table 3.1 Coordinates of peak in the a_p-Ω_p diagram for control parameter V_{mP} and certain value of α

α	$a_{P'}$	$\Omega_{P'}$	$V_{mP'}$	V_{mP}
4/3	1.5667	1.0445	1.3941	1.4000
5/3	1.6764	1.1176	1.4917	1.4970

procedure. We note that there is a hysteresis in diagrams in the region P-Q-R-S (see Fig. 3.6), where two stable steady-state responses exist. This phenomena, called Sommerfeld effect, depends on the orders of nonlinearity α.

Using relations (3.81)–(3.83) coordinates of peaks ($a_{P'}$, $\Omega_{P'}$) in the diagram (3.77) and corresponding control parameters $V_{mP'}$ are calculated and shown in Table 3.1. Approximate values $V_{mP'}$ are compared with the exact numerically obtained value V_{mP}. It can be seen that they are in good agreement.

For the value of the control parameter V_{mP} the amplitude-frequency curve (3.78) represents the boundary for which the Sommerfeld effect exists.

The question is whether the Sommerfeld effect in this non-ideal system can be suppressed. Using the procedure given in this section, the value of the parameter α for which the Sommerfeld effect is suppressed can be calculated. For the driving torque with cubic nonlinearity ($n = 3$) the relation (3.85) simplifies to

$$\frac{4\zeta_1}{1-\alpha} = \zeta_1 + 3C_m\mu_1 \left(\frac{2}{\eta_1}\right)^{\frac{1}{3}} \left(\frac{\zeta_1}{\mu_1}\right)^{\frac{4}{3}}. \tag{3.100}$$

Substituting the previously mentioned parameter values and $C_m = 1$ into (3.100) we obtain the critical value of the order of nonlinearity

$$\alpha^* = 0.59851. \tag{3.101}$$

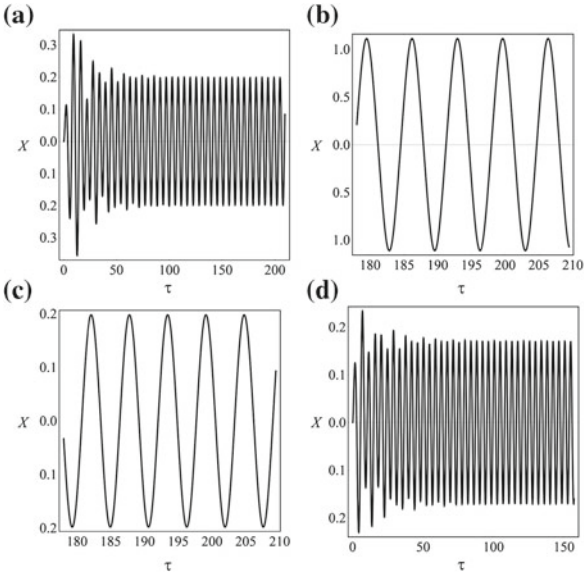

Fig. 3.7 Time history diagrams for $\alpha = 5/3$: **a** non-stationary diagram for $V_m = 1.2$; **b**, **c** Steady-state diagrams for $V_m = 1.2$; **d** non-stationary motion for $V_m = 1.4$

For $\alpha = \alpha^*$ the Sommerfeld effect is suppressed. It means, that for all values of $\alpha \geq 1$ the Sommerfeld effect exists.

To prove the correctness of analytically and numerically obtained results, let us plot curves for the steady-state and of the non-stationary motion. In Fig. 3.7, amplitude-frequency diagrams of the oscillator with nonlinearity order $\alpha = 5/3$ for the control parameter $V_m = 1.2$ (non-stationary motion in Fig. 3.7a and two steady-state motions in Fig. 3.7b, c) and for the control parameter $V_m = 1.4$ (non-stationary motion in Fig. 3.7d) are shown. Comparing these diagrams with values shown in Fig. 3.7, it can be seen that they are in good agreement.

Based on the obtained results, it can be concluded that the methods developed for the general type of the non-ideal system (mentioned in the previous sections) are applicable for the pure nonlinear oscillator coupled with a non-ideal source excited with the nonlinear torque.

3.3 Pure Strong Nonlinear Oscillator and a Non-ideal Energy Source

Let us consider a non-ideal energy source which is settled on a foundation which is a nonlinear oscillator (Fig. 3.4) The elastic characteristic of the oscillator is pure nonlinear and described with an elastic force which is proportional to the displacement x with the positive rational exponent $\alpha \in \mathbb{R}$ (integer or noninteger)

$$F_e = kx\,|x|^{\alpha-1}, \tag{3.102}$$

where k is the rigidity constant. The damping property of the system is supposed to be a linear velocity function and is given with the damping force

$$F_d = c\dot{x}, \tag{3.103}$$

where c is the damping coefficient.

The oscillator is driven by a motor which has an unbalance m which is on the distance d to the rotor shaft. Position of the unbalance is varying in time and is described with the angle φ. As it is suggested in Dantas and Balthazar (2003), Tsuchida et al. (2003, 2005), Souza et al. (2005a, b), Felix et al. (2009a), Castao et al. (2010), the motor torque is a linear function of angular velocity

$$\mathcal{M}(\dot{\varphi}) = V_{\varphi m} - C_{\varphi m}\dot{\varphi}, \tag{3.104}$$

where $C_{\varphi m}$ and $V_{\varphi m}$ are constant values and $\dot{\varphi}$ is the angular velocity of the motor. The system executes a rectilinear motion and the displacement is given with the variable x. This motion has an effect on the rotation of the rotor of the motor.

The suggested oscillator-motor system has two-degrees-of-freedom. The two generalized coordinates are x and φ. In general, the Lagrange differential equations of motion for the system are

$$\begin{aligned} \frac{d}{dt}\frac{\partial T}{\partial \dot{x}} - \frac{\partial T}{\partial x} + \frac{\partial U}{\partial x} + \frac{\partial \Phi}{\partial \dot{x}} &= Q_x, \\ \frac{d}{dt}\frac{\partial T}{\partial \dot{\varphi}} - \frac{\partial T}{\partial \varphi} + \frac{\partial U}{\partial \varphi} + \frac{\partial \Phi}{\partial \dot{\varphi}} &= Q_\varphi, \end{aligned} \tag{3.105}$$

where T is the kinetic energy, U is the potential energy, Φ is the dissipation function and Q_x and Q_φ are the corresponding generalized forces.

The kinetic energy, potential energy and the dissipation function are, respectively,

$$T = \frac{1}{2}M\dot{x}^2 + \frac{1}{2}m(\dot{x} - d\dot{\varphi}\cos\varphi)^2 + \frac{1}{2}m(d\dot{\varphi}\sin\varphi)^2 + \frac{1}{2}J\dot{\varphi}^2, \tag{3.106}$$

$$U = \frac{k}{\alpha+1}x^{\alpha+1}, \qquad \Phi = \frac{1}{2}c\dot{x}^2, \tag{3.107}$$

where a dot denotes differentiation with respect to time t, M is mass of the oscillator, J is the moment of inertia of the motor rotor, m is mass of the rotor unbalance and d is the length of the rotor unbalance. The virtual work of the motor torque is

$$\delta A = \mathcal{M}(\dot{\varphi})\delta\varphi, \tag{3.108}$$

and the generalized forces

$$Q_x = 0, \quad Q_\varphi = \mathcal{M}(\dot{\varphi}). \tag{3.109}$$

Substituting (3.106)–(3.109) into (3.105), the mathematical model of the system is obtained (Cveticanin 2009)

$$\begin{aligned} \ddot{x}(M+m) + kx\,|x|^{\alpha-1} + c\dot{x} - md(\ddot{\varphi}\cos\varphi - \dot{\varphi}^2\sin\varphi) = 0, \\ (J+md^2)\ddot{\varphi} - md\ddot{x}\cos\varphi = \mathcal{M}(\dot{\varphi}). \end{aligned} \tag{3.110}$$

In this case the effect of gravitational force is omitted. The model (3.110) represents a system of two coupled strong nonlinear second order differential equations. To find the exact (closed form) solution of (3.110) is even impossible. An approximate solving procedure for the resonant motion of the system is suggested. It is based on the averaging procedure adopted for the system (3.110). The influence of the nonlinearity order on the Sommerfeld effect is discussed. A method for suppressing Sommerfeld effect is developed. The critical parameters for the Sommerfeld phenomena are approximately determined. As examples the steady-state resonant motions of the oscillators with non-integer order driven by a non-ideal force are considered.

3.3.1 Model of the System

It is convenient to normalize the coordinates and time in (3.110) according to

$$x \longrightarrow y = x/l, \qquad t \longrightarrow \tau = \Omega^* t, \tag{3.111}$$

where l is the initial length of the non-deformed spring and Ω^* is the synchronous angular velocity of the rotor (see Dimentberg et al. 1997). By introducing (3.111) and the notation $\phi \to \psi_1$, the differential equations (3.110)) transform into

$$\begin{aligned} y'' + \zeta y' + p^2 y\,|y|^{\alpha-1} = \mu(\varphi''\cos\varphi - \varphi'^2\sin\varphi), \\ \varphi'' = \eta y''\cos\varphi + (V_m^* - C_m^*\varphi'), \end{aligned} \tag{3.112}$$

where

$$\begin{aligned} p^2 &= \frac{kl^{\alpha-1}}{\Omega^{*2}(M+m)}, \qquad \zeta = \left(\frac{c}{M+m}\right)\frac{1}{\Omega^*}, \qquad \mu = \frac{dm}{l(M+m)}, \\ \eta &= \frac{dml}{J+md^2}, \qquad V_m^* = \frac{V_{\varphi m}}{(J+md^2)\Omega^{*2}}, \qquad C_m^* = \frac{C_{\varphi m}}{(J+md^2)\Omega^*}, \end{aligned} \tag{3.113}$$

and $(') \equiv (\mathrm{d}/\mathrm{d}\tau)$, $('') \equiv (\mathrm{d}^2/\mathrm{d}\tau^2)$. After some modification, we have

$$y''(1-\mu\eta\cos^2\varphi)+p^2y\,|y|^{\alpha-1}+\zeta y'=\mu\left[(V_m^*-C_m^*\varphi')\cos\varphi-\varphi'^2\sin\varphi\right],$$
$$\varphi''(1-\mu\eta\cos^2\varphi)+\mu\eta\varphi'^2\cos\varphi\sin\varphi=-\eta(\zeta y'+p^2y\,|y|^{\alpha-1})\cos\varphi+(V_m^*-C_m^*\varphi'). \tag{3.114}$$

Due to the physical properties of the system, it can be concluded that the parameters μ and η are small in comparison to 1 and can be treated as the product of a small parameter ε and constants μ_1 and η_1, i.e., $\mu=\varepsilon\mu_1$ and $\eta=\varepsilon\eta_1$. The same is valid for V_m^* and C_m^*, and also the damping parameter ζ, i.e., we have $V_m^*=\varepsilon V_m$, $C_m^*=\varepsilon C_m$ and $\zeta=\varepsilon\zeta_1$. Then, the system of differential equations (3.114) is simplified into

$$y''+p^2y\,|y|^{\alpha-1}=-\varepsilon(\mu_1\varphi'^2\sin\varphi+\zeta_1y'),$$
$$\varphi''=-\varepsilon\eta_1p^2y\,|y|^{\alpha-1}\cos\varphi+\varepsilon V_m(1-K_m\varphi'), \tag{3.115}$$

where $\varepsilon<<1$ is a small positive parameter and $K_m=C_m/V_m$. In (3.115) the small terms of the second order are neglected. The Eq. (3.115) represent the system of two coupled differential equations which describe the motion of the non-ideal system given in Cveticanin and Zukovic (2015a).

3.3.2 *Analytical Solving Procedure*

Let us rewrite the differential equations (3.115) into a system of four first order differential equations

$$\begin{aligned}y'&=z,\\ z'&=-p^2y\,|y|^{\alpha-1}+\varepsilon F_1,\\ \varphi'&=\Omega,\\ \Omega'&=\varepsilon F_2,\end{aligned} \tag{3.116}$$

where

$$F_1=-(\mu_1\Omega^2\sin\varphi+\zeta z),\qquad F_2=V_m(1-K_m\Omega)-\eta_1p^2y\,|y|^{\alpha-1}\cos\varphi. \tag{3.117}$$

For $\varepsilon=0$, the Eq. (3.116) transform into

$$y'=z,\qquad z'=-p^2y\,|y|^{\alpha-1},\qquad \varphi'=\Omega,\qquad \Omega'=0. \tag{3.118}$$

The first two differential equations describe the motion of a pure integer or noninteger order nonlinear oscillator (see Cveticanin et al. 2012; Cveticanin and Pogany 2012). The exact analytical solution of (3.118) is

$$y = a\mathrm{ca}(\alpha, 1, \nu t), \qquad z = -\frac{2ha^{(\alpha+1)/2}}{\alpha+1}\mathrm{sa}(1, \alpha, \nu t),$$
$$\varphi = C_1 t + C_2, \qquad \Omega = C_1, \tag{3.119}$$

where

$$\nu = ha^{(\alpha-1)/2}, \qquad h = |p|\sqrt{\frac{\alpha+1}{2}}, \tag{3.120}$$

C_1 and C_2 are constants of integration, A is an arbitrary constant and $\mathrm{ca}(\alpha, 1, \nu t) = \mathrm{ca}$ and $\mathrm{sa}(1, \alpha, \nu t) = \mathrm{sa}$ are the cosine and sine Ateb-functions given by Droniuk et al. (1997, 2010), Droniuk and Nazarkevich (2010) (see Appendix). Namely, (3.119) is the generating solution of the generating Eq. (3.118). Based on that solution, the trial solution for (3.116) is introduced.

Let us express y, z, φ and Ω as functions of new variables a, ψ, φ and Ω, i.e.

$$y = a\mathrm{ca}(\alpha, 1, \psi) \equiv a\mathrm{ca}(\psi),$$
$$z = -\frac{2h}{\alpha+1}a^{(\alpha+1)/2}\mathrm{sa}(1, \alpha, \psi) \equiv -\frac{2h}{\alpha+1}a^{(\alpha+1)/2}\mathrm{sa}(\psi), \tag{3.121}$$

and $\psi_2 \to \Theta$. According to the expressions for the derivatives of Ateb functions (A22) and (A23) (see Appendix), the first time derivatives of (3.121) follow

$$y' = a'\mathrm{ca}(\psi) - \frac{2\psi'}{\alpha+1}a\mathrm{sa}(\psi),$$
$$z' = -ha^{(\alpha-1)/2}A'\mathrm{sa}(\psi) - \frac{2h\psi'}{\alpha+1}a^{(\alpha+1)/2}\mathrm{ca}^{\alpha}(\psi). \tag{3.122}$$

Substituting (3.122) into (3.116) and using the relations (A21) (see Appendix) and (3.120), the modified equations of motion are

$$\psi' = ha^{(\alpha-1)/2} - \varepsilon F_1\frac{\alpha+1}{2h}a^{-(\alpha+1)/2}\mathrm{ca}(\psi),$$
$$a' = -\frac{\varepsilon F_1}{h}a^{(1-\alpha)/2}\mathrm{sa}(\psi),$$
$$\varphi' = \Omega,$$
$$\Omega' = \varepsilon F_2, \tag{3.123}$$

where

$$F_1 = -\mu_1\Omega^2\sin\varphi + \zeta_1\frac{2h}{\alpha+1}a^{(\alpha+1)/2}\mathrm{sa}(\psi),$$
$$F_2 = V_m(1 - K_m\Omega) - \eta_1 p^2 a\mathrm{ca}(\psi)\,|a\mathrm{ca}(\psi)|^{\alpha-1}\cos\varphi.$$

Equation (3.123) are the four first order differential equations which in the first approximation correspond to (3.166). In these equations the trigonometric and Ateb periodic functions exist. It is well known that the period of trigonometric functions $\sin\varphi$ and $\cos\varphi$ is 2π, while of the Ateb functions $\mathrm{sa}(\psi)$ and $\mathrm{ca}(\psi)$ is $2\Pi_\alpha$, where the expression for Π_α is given in Appendix (see Eq. (A14))

$$\Pi_\alpha = \mathrm{B}\left(\frac{1}{\alpha+1}, \frac{1}{2}\right), \tag{3.124}$$

and B is the beta function (Abramowitz and Stegun 1964). Introducing the new variable

$$\psi = \frac{\Pi_\alpha}{2\pi}\bar{\psi}, \tag{3.125}$$

we obtain the Ateb functions $\mathrm{sa}(\frac{\Pi_\alpha}{2\pi}\bar{\psi})$ and $\mathrm{ca}(\frac{\Pi_\alpha}{2\pi}\bar{\psi})$ whose period is also 2π as is for the trigonometric functions $\sin\varphi$ and $\cos\varphi$. Substituting (3.125) into (3.123), it follows

$$\begin{aligned}
\bar{\psi}' &= \left(\frac{2\pi}{\Pi_\alpha}\right) h a^{(\alpha-1)/2} - \varepsilon F_1 \frac{\alpha+1}{2h}\left(\frac{2\pi}{\Pi_\alpha}\right) a^{-(\alpha+1)/2}\mathrm{ca}\left(\frac{\Pi_\alpha}{2\pi}\bar{\psi}\right),\\
a' &= -\frac{\varepsilon F_1}{h} a^{(1-\alpha)/2}\mathrm{sa}\left(\frac{\Pi_\alpha}{2\pi}\bar{\psi}\right),\\
\varphi' &= \Omega,\\
\Omega' &= \varepsilon F_2,
\end{aligned} \tag{3.126}$$

where

$$F_1 = -\mu_1\Omega^2\sin\varphi + \zeta_1\frac{2h}{\alpha+1}a^{(\alpha+1)/2}\mathrm{sa}\left(\frac{\Pi_\alpha}{2\pi}\bar{\psi}\right),$$

$$F_2 = V_m\left(1 - K_m\Omega\right) - \eta_1 p^2 A\mathrm{ca}\left(\frac{\Pi_\alpha}{2\pi}\bar{\psi}\right)\left|a\mathrm{ca}\left(\frac{\Pi_\alpha}{2\pi}\bar{\psi}\right)\right|^{\alpha-1}\cos\psi. \tag{3.127}$$

Differential equations (3.126) represent the mathematical model of the non-ideal system for the non-resonant case which is not of a significant interest. Much more important case is the resonant one.

3.3.3 *Resonant Case and the Averaging Solution Procedure*

Let us introduce the new variable θ which satisfies the relation

$$\bar{\psi} = \theta + \varphi, \tag{3.128}$$

with time derivative

$$\bar{\psi}' = \theta' + \Omega. \tag{3.129}$$

Substituting (3.129) and (3.128) into (3.126), differential equations with variables A, θ, φ and Ω follow as

$$\begin{aligned}
\theta' &= \left[\left(\frac{2\pi}{\Pi_\alpha}\right) h a^{(\alpha-1)/2} - \Omega\right] - \varepsilon F_1 \frac{\alpha+1}{2h}\left(\frac{2\pi}{\Pi_\alpha}\right) a^{-(\alpha+1)/2} \mathrm{ca}\left(\frac{\Pi_\alpha}{2\pi}(\theta+\varphi)\right), \\
a' &= -\frac{\varepsilon F_1}{h} a^{(1-\alpha)/2} \mathrm{sa}\left(\frac{\Pi_\alpha}{2\pi}(\theta+\varphi)\right), \\
\varphi' &= \Omega, \\
\Omega' &= \varepsilon F_2,
\end{aligned} \tag{3.130}$$

where

$$\begin{aligned}
F_1 &= -\mu_1 \Omega^2 \sin\varphi + \gamma \frac{2h}{\alpha+1} a^{(\alpha+1)/2} \mathrm{sa}\left(\frac{\Pi_\alpha}{2\pi}(\theta+\varphi)\right), \\
F_2 &= V_m(1 - K_m\Omega) - \eta_1 p^2 a \mathrm{ca}\left(\frac{\Pi_\alpha}{2\pi}(\theta+\psi_1)\right) \left|a\mathrm{ca}\left(\frac{\Pi_\alpha}{2\pi}(\theta+\varphi)\right)\right|^{\alpha-1} \cos\varphi.
\end{aligned} \tag{3.131}$$

For the case when

$$\left(\frac{2\pi}{\Pi_\alpha}\right) h a^{(\alpha-1)/2} - \Omega = \varepsilon\sigma, \tag{3.132}$$

the condition of nonlinear resonance is satisfied. Thus, according to $(3.130)_1$, θ' is of the order ε. For θ' of the order $O(\varepsilon)$, the relation (3.129) yields the difference between the frequencies $(\bar{\psi}' - \varphi') \equiv (\bar{\psi}' - \Omega)$ to be also of the ε order.

To solve the system of differential equations (3.130) is not an easy task. It is the reason the averaging procedure suggested by Zhuravlev and Klimov (1988) is adopted for this special case. The averaging is done over the period 2π of the variable φ. The averaged differential equations are

$$\begin{aligned}
\theta' &= \left[\left(\frac{2\pi}{\Pi_\alpha}\right) h a^{(\alpha-1)/2} - \Omega\right] - \varepsilon \bar{F}_{1\theta} \frac{\alpha+1}{2h}\left(\frac{2\pi}{\Pi_\alpha}\right) a^{-(\alpha+1)/2}, \\
a' &= -\frac{\varepsilon \bar{F}_{1A}}{h} a^{(1-\alpha)/2}, \\
\varphi' &= \Omega, \qquad \Omega = \varepsilon \bar{F}_2,
\end{aligned} \tag{3.133}$$

where

$$\bar{F}_{1A} = -\mu_1 \Omega^2 \bar{f}_1 + \zeta_1 \frac{2h}{\alpha+1} a^{(\alpha+1)/2} \bar{f}_2,$$
$$\bar{F}_{1\theta} = -\mu_1 \Omega^2 \bar{f}_3 + \zeta_1 \frac{2h}{\alpha+1} a^{(\alpha+1)/2} \bar{f}_4,$$
$$\bar{F}_2 = V_m(1 - K_m \Omega) - \eta_1 p^2 A^\alpha \bar{f}_5, \tag{3.134}$$

and

$$\bar{f}_1 = \frac{1}{2\pi} \int_0^{2\pi} \sin\varphi \mathrm{sa}\left(\frac{\Pi_\alpha}{2\pi}(\theta+\varphi)\right) d\varphi, \quad \bar{f}_2 = \frac{1}{2\pi} \int_0^{2\pi} \mathrm{sa}^2\left(\frac{\Pi_\alpha}{2\pi}(\theta+\varphi)\right) d\varphi,$$
$$\bar{f}_3 = \frac{1}{2\pi} \int_0^{2\pi} \sin\varphi \mathrm{ca}\left(\frac{\Pi_\alpha}{2\pi}(\theta+\varphi)\right) d\varphi,$$
$$\bar{f}_4 = \frac{1}{2\pi} \int_0^{2\pi} \mathrm{sa}\left(\frac{\Pi_\alpha}{2\pi}(\theta+\varphi)\right) \mathrm{ca}\left(\frac{\Pi_\alpha}{2\pi}(\theta+\varphi)\right) d\varphi,$$
$$\bar{f}_5 = \frac{1}{2\pi} \int_0^{2\pi} \cos\varphi \mathrm{ca}\left(\frac{\Pi_\alpha}{2\pi}(\theta+\varphi)\right) \left|\mathrm{ca}^{\alpha-1}\left(\frac{\Pi_\alpha}{2\pi}(\theta+\varphi)\right)\right| d\varphi. \tag{3.135}$$

Being the sine and cosine Ateb periodic functions, they are suitable for Fourier series expansion. The finite Fourier approximation of the functions is according to Droniuk et al. (2010, 2010)

$$\mathrm{sa}(1,\alpha,\psi) = \frac{a_0}{2} + \sum_{n=1}^{\infty} a_n \sin\frac{\pi n\psi}{\Pi_\alpha},$$
$$\mathrm{ca}(\alpha,1,\psi) = \sum_{n=1}^{\infty} b_n \cos\frac{\pi n\psi}{\Pi_\alpha}, \tag{3.136}$$

where the coefficient in the series are

$$a_0 = \frac{2}{\Pi_\alpha} \int_0^{\Pi_\alpha} sa(1,\alpha,\psi) d\psi, \qquad a_n = \frac{2}{\Pi_\alpha} \int_0^{\Pi_\alpha} sa(1,\alpha,\psi) \sin\frac{\pi n\psi}{\Pi_\alpha} d\psi,$$
$$b_n = \frac{2}{\Pi_\alpha} \int_0^{\Pi_\alpha} ca(\alpha,1,\psi) \cos\frac{\pi n\psi}{\Pi_\alpha} d\psi \tag{3.137}$$

and $\psi \equiv \frac{\Pi_\alpha}{2\pi}(\theta+\varphi)$. In this calculation the Fourier series expansion of the function $\mathrm{ca}(\psi)\left|\mathrm{ca}^{\alpha-1}(\psi)\right|$ is also introduced as (see Mickens 2004; Cveticanin 2008)

$$ca(\psi)\left|\mathrm{ca}^{\alpha-1}(\psi)\right| = \sum_{n=1}^{\infty} c_n \cos(n\psi), \tag{3.138}$$

with

$$c_n = \frac{4}{\pi}\int_0^{\pi/2} ca(\psi)\left|\mathrm{ca}^{\alpha-1}(\psi)\right|\cos(n\psi)d\psi. \tag{3.139}$$

For practical reasons, it is suitable to determine the solution in the first approximation. Then, using the first terms of the Fourier series (3.136), the expressions (3.134) and (3.135) are transformed into

$$\bar{f}_1 = \frac{1}{2}a_1\cos\theta, \quad \bar{f}_2 = \frac{1}{2}a_1^2, \quad \bar{f}_3 = -\frac{1}{2}b_1\sin\theta, \quad \bar{f}_4 = 0, \quad \bar{f}_5 = \frac{1}{2}c_1\cos\theta, \tag{3.140}$$

and

$$\begin{aligned}\bar{F}_{1A} &= -\frac{1}{2}\mu_1 a_1\Omega^2\cos\theta + \zeta_1\frac{h}{\alpha+1}a^{(\alpha+1)/2}a_1^2,\\ \bar{F}_{1\theta} &= \frac{1}{2}\mu_1 b_1\Omega^2\sin\theta, \quad \bar{F}_2 = V_m(1-K_m\Omega) - \frac{1}{2}\eta_1 p^2 a^\alpha c_1\cos\theta\end{aligned} \tag{3.141}$$

where a_1, b_1 and c_1 are the coefficients calculated according to (3.137) and (3.139) for $n = 1$. Substituting (3.141) into (3.133) the simplified averaged differential equations are

$$\begin{aligned}\theta' &= \left[\left(\frac{2\pi}{\Pi_\alpha}\right)ha^{(\alpha-1)/2} - \Omega\right] - \frac{\varepsilon\mu_1}{2}b_1\Omega^2\frac{\alpha+1}{2h}\left(\frac{2\pi}{\Pi_\alpha}\right)a^{-(\alpha+1)/2}\sin\theta,\\ A' &= -\frac{1}{h}a^{(1-\alpha)/2}\left(-\frac{\varepsilon\mu_1}{2}a_1\Omega^2\cos\theta + \varepsilon\zeta_1 a_1^2\frac{h}{\alpha+1}a^{(\alpha+1)/2}\right),\\ \Omega' &= \varepsilon\left(V_m(1-K_m\Omega) - \frac{1}{2}\eta_1 c_1 p^2 a^\alpha\cos\theta\right).\end{aligned} \tag{3.142}$$

The equations describe the transient motion in the resonant case.

Steady - state solution

Equating the right side of the Eq. (3.142) to zero and after some modification the steady-state equations up to the first order approximation are

$$\varepsilon\mu_1\Omega^2\sin\theta = \frac{1}{b_1}\frac{4h}{\alpha+1}\left[ha^{(\alpha-1)/2} - \left(\frac{\Pi_\alpha}{2\pi}\right)\Omega\right]a^{(\alpha+1)/2}, \tag{3.143}$$

$$\varepsilon\mu_1\Omega^2\cos\theta = \frac{2\varepsilon\zeta_1 a_1 h}{\alpha+1}a^{(\alpha+1)/2}, \tag{3.144}$$

$$\eta_1 c_1 p^2 a^\alpha \cos\theta = 2V_m(1 - K_m\Omega). \tag{3.145}$$

Eliminating the variable θ in the Eqs. (3.143) and (3.144) the frequency - response relation is as follows

$$1 = \frac{a^{(\alpha+1)}}{\Omega^4\mu_1^2}\left(\left(\frac{2\zeta_1 a_1 h}{\alpha+1}\right)^2 + \left(\frac{4h}{\varepsilon b_1}\frac{ha^{(\alpha-1)/2} - \left(\frac{\Pi_\alpha}{2\pi}\right)\Omega}{\alpha+1}\right)^2\right). \tag{3.146}$$

Dividing Eqs. (3.144) and (3.145) the $a - \theta$ expression as a function of the control parameter V_m is obtained

$$V_m(1 - K_m\Omega) = \frac{\eta_1 c_1 a_1 p^2}{\mu_1(\alpha+1)}\frac{\zeta_1 h}{\Omega^2}a^{(3\alpha+1)/2}. \tag{3.147}$$

Characteristic points

The characteristic point P for the curves (3.72) and (3.147) corresponds to the peak amplitude and exists if the condition of the equality of the gradients $da/d\Omega$ for the both curves is satisfied. Due to complexity of the expressions, it is suggested to use the approximate procedure for obtaining of this point. Instead of the exact characteristic point P, the point P' is determined, in which the bifurcation of the solutions of the Eq. (3.72) appears. It is known that the locus of these two points (P and P') are quite close to each other.

Let us assume that in (3.66) the left hand side of the equation is zero, i.e.,

$$ha^{(\alpha-1)/2} - \left(\frac{\Pi_\alpha}{2\pi}\right)\Omega = 0. \tag{3.148}$$

Substituting (3.148) into (3.72) the peak amplitude is obtained

$$a_P = \left(\frac{1}{\mu_1}\left(\frac{\Pi_\alpha}{2\pi h}\right)^2\left(\frac{2\zeta_1 a_1 h}{\alpha+1}\right)\right)^{2/(\alpha-3)}. \tag{3.149}$$

Substituting (3.149) into (3.148), the locus Θ_P for a_P is obtained

$$\Omega_P = \left(\left(\frac{\Pi_\alpha}{2\pi h}\right)^{(\alpha+1)}\left(\frac{2\zeta_1 a_1 h}{\mu_1(\alpha+1)}\right)^{(\alpha-1)}\right)^{1/(\alpha-3)}. \tag{3.150}$$

Equations (3.149) and (3.150) with (3.147) give the value of a control parameter $V_{mP'}$ of the motor torque

$$V_{mP} = \frac{q_2 c_1 a_1 p^2}{\mu_1(\alpha+1)(1 - K_m\Omega_P)}\frac{\zeta_1 h}{\Omega_P^2}a_P^{(3\alpha+1)/2}. \tag{3.151}$$

For this approximate value of the control parameter V_{mP} the Sommerfeld effect has to appear.

Analyzing the relations (3.149) and (3.150) it can be seen that the relations are independent on the value of η_1.

3.3.4 Suppression of the Sommerfeld Effect

As it is previously shown the Eqs. (3.149)–(3.151) give us the values $a_{P'}$, $\Omega_{P'}$ of the point P' and also the corresponding control parameter V_{mP} for which the Sommerfeld effect exists and the amplitude-frequency torque curve is forced through the point P'. Our intention is to suppress the Sommerfeld effect which is evident for P'.

Let us calculate the gradient of the backbone curve (3.148) in the bifurcation point P. Substituting a_P given with the relation (3.149) into the first derivative $(da/d\Omega)$ of the relation (3.148), the required gradient is obtained

$$\left(\frac{da}{d\Omega}\right)_P = \frac{\alpha+1}{\alpha-1}\frac{\mu_1}{\zeta_1 a_1}\left(\frac{2\pi}{\Pi_\alpha}\right). \tag{3.152}$$

The gradient is the function of the order of the nonlinearity α. For $\alpha < 1$ the direction of the tangent is such to give an obtuse angle and for $\alpha > 1$ a sharp angle. For $\alpha = 1$ the tangent is orthogonal.

The gradient of the amplitude-frequency torque curve (3.147) for the bifurcation point is also worth to be determined. The first derivative $(dA/d\Omega)$ for (3.147) is calculated and the coordinates Ω_P for a_P given with relations (3.149) and (3.150) have to be substituted

$$\left(\frac{da}{d\Omega}\right)_P = V_{mP}\frac{2(2-3K_m\Omega_P)\mu_1}{\eta_1 c_1 a_1 p^2 \zeta_1 h}\frac{\alpha+1}{3\alpha+1}\frac{\Omega_P}{(a_P)^{(3\alpha-1)/2}}. \tag{3.153}$$

Equating the gradients (3.152) and (3.153) in the P' and assuming the condition (3.151), we have

$$\frac{3\alpha+1}{\alpha-1}\frac{\mu_1}{\zeta_1 a_1}\left(\frac{2\pi}{\Pi_\alpha}\right) = \frac{2(2-3K_m\Omega_P)}{(\alpha+1)(1-K_m\Omega_P)}\frac{a_P}{\Omega_P}. \tag{3.154}$$

The relation (3.154) depends on the parameter of the torque K_m, parameters of eccentricity μ_1, and also on the order of nonlinearity α. Due to the motor properties (3.3) and the sign of the gradient of the V_m curve, it can be concluded that the relation (3.154) is valid only for $\alpha < 1$.

Let us solve the relation (3.154) for the driving parameter

$$\tilde{K}_m = \frac{2-p_1}{(3-p_1)\Omega_P}, \tag{3.155}$$

where

$$p_1 = \frac{(3\alpha+1)(\alpha+1)}{\alpha-1}\frac{\mu_1}{\zeta_1 a_1}\left(\frac{\pi}{\Pi_\alpha}\right)\frac{\Omega_P}{a_P}. \tag{3.156}$$

Then the value $\tilde{V}_m$ is the necessary one for elimination of the Sommerfeld effect. Substituting the value of $\tilde{K}_m$ (3.155) into the relation for V_{mP} (3.151), the corresponding control parameter $\tilde{V}_m$ is obtained

$$\tilde{V}_m = \frac{(3-p_1)\eta_1 c_1 a_1 p^2}{\mu_1(\alpha+1)}\frac{\zeta_1 h}{\Omega_P^2}a_P^{(3\alpha+1)/2}. \tag{3.157}$$

Finally, the parameter $\tilde{C}_m$ is

$$\tilde{C}_m = \frac{\tilde{V}_m}{\tilde{K}_m} = \frac{\eta_1 c_1 a_1 p^2(3-p_1)^2}{\mu_1(\alpha+1)(2-p_1)}\frac{\zeta_1 h}{\Omega_p}a_P^{(3\alpha+1)/2}. \tag{3.158}$$

For the parameter value (3.158) i.e., (3.155) and (3.157) the jump phenomena in the non-ideal system with known order of nonlinearity α is excluded. For all values of the control parameter V_m there is always only one steady point in the $a-\Omega$ curve, i.e., only one intersection point between V_m and $a-\Omega$ curve. Then, the Sommerfeld effect does not exist.

3.3.5 *Numerical Examples of Non-ideal Driven Pure Nonlinear Oscillators*

For physical interpretation, a motor-support system mounted in a soya extraction plant is considered: mass of the system is $(M+m)$ of 5 kg, radius of the motor rotor is 0.120 m, measure of the unbalance is $md = 0.0125$ kgm, length l is 0.05 m, moment of inertia of the motor rotor $J = 0.698 \times 10^{-3}$ kgm^2, the synchronous speed of the rotor is $\Omega^* = 1450$ rpm and the damping coefficient is $c = 37.961$ kg/s. The three types of nonlinearity are considered: one, with the order of nonlinearity $\alpha = 2/3$ (smaller than 1) and coefficient of rigidity $k = 0.42470 \times 10^5$ N/m$^{2/3}$, second, with $\alpha = 1$ (linear case) and coefficient of rigidity $k = 1.152\,8 \times 10^5$ N/m and with the order of nonlinearity $\alpha = 5/3$ (higher than 1) and coefficient of rigidity $k = 8.494\,1 \times 10^5$ N/m$^{5/3}$. Two values of the motor parameters are considered: $C_{\varphi m} = 1.898$ Nm/s and $C_{\varphi m} = 18.98$ Nm/s. The corresponding non-dimensional parameters are according to (3.53): $\varepsilon = 0.1$, $\mu_1 = 0.5$, $\eta_1 = 0.5$, $p^2 = 1$ and $\zeta_1 = 0.5$. Two values for C_m are 1 and 10. Varying the control parameter V_m of the motor, the steady-state properties of the system are analyzed. For $C_m = 1$ the initial control parameter for the increasing case is $V_m = 0.3$ and for the decreasing case it is $V_m = 1.2$, while for $C_m = 10$ it is $V_m = 3$ and $V_m = 12$, respectively. The analytical results are obtained by solving the relations (3.72) and (3.147), and numerical ones by

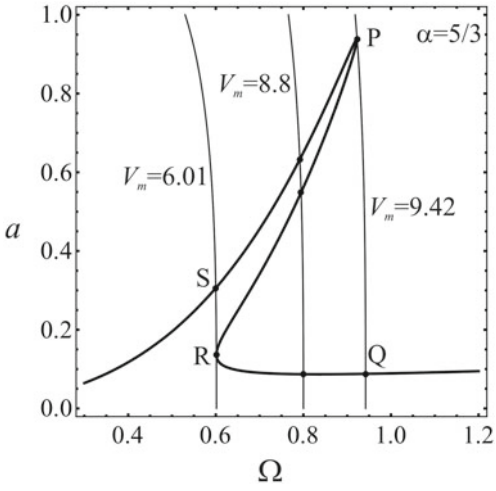

Fig. 3.8 Frequency-response steady state curve obtained analytically for $\alpha = 5/3$ and $C_m = 10$ with characteristic points

integrating of the original differential equations of motion (3.48). For numerical calculation the Runge–Kutta procedure is applied.

The numerical procedure is as follows: for a certain value of the control parameter V_m the relations (3.48) are numerically solved and the amplitude and frequency are computed. The amplitude of vibration is computed for the maximal disposition of the oscillator from the equilibrium position, while the frequency of vibration is the averaged value for $\dot{\psi}_1$ during the steady state motion. These values are the initial values for the further numerical calculation. Increasing the control parameter V_m for a small value, the new steady-state parameters are computed. The numerical calculation is repeated for the new higher value of the control parameter and with initial conditions which are the previous steady-state parameters. After the significant repetition of the numerical process for increasing of the control parameter V_m, an amplitude-frequency curve for increasing of the control parameter is obtained. In contrary, if the same procedure is applied but the control parameter is decreased the another amplitude-frequency curve is obtained which partly differs from the first one.

If during the numerical solution of (3.48) the obtained amplitudes significantly differ for the two infinitesimal close values of the control parameter V_m, it is evident that the jump phenomena occurs. It gives us the chance to "recognized" the Sommerfeld effect during the numerical process.

In Figs. 3.8 and 3.9 the amplitude - frequency diagrams obtained analytically by solving (3.72) and (3.147) and numerically by solving (3.48) for $C_m = 10$ and $\alpha = 5/3$ are plotted. The control parameter V_m is varied and the steady-state amplitude - frequency values are obtained. The computation time was 200 periods of vibration T. The steady-state numerical solution is reached after approximately $30T$. The period T is computed numerical. For the certain value of control parameter V_m the steady state amplitude and frequency are calculated. These values were used as the

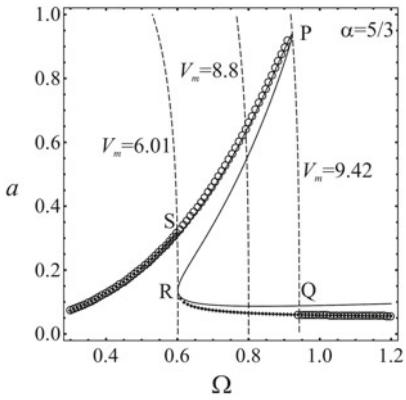

Fig. 3.9 Frequency-response curves for $\alpha = 5/3$ and $C_m = 10$ obtained analytically (*full line*) and numerically (*circles* - for the increasing of V_m, *squares* - for decreasing of V_m)

initial conditions for computation of the steady-state values for the new value of the control parameter V_m.

From the both figures it is obvious that for slow increasing of Ω and variation of the motor parameter V_m, the amplitude of vibration increases up to the point P. Using the relations (3.149)–(3.151) the parameters of the characteristic point are obtained: $a_P = 0.9$, $\Omega_P = 0.92$ and $V_{mP} = 9.42$. Along the curve V_{mP} the jump phenomena from P to Q ($a_Q = 0.098$, $\Omega_Q = 0.94$) occurs. For that position $\Omega_Q > \Omega_P$, but the amplitude a_Q is significantly smaller than a_P. Further increase of the control parameter V_m causes the further decrease of the amplitude of vibration for increase of the frequency Ω. If the value of the control parameter V_m is decreased, the steady-state locus in $a - \Omega$ plane moves to left along the $a - \Omega$ curve to the point R. The frequency Ω decreases and the amplitude a increases slowly up to the value of $a_R = 0.1$ at the frequency $\Omega_R = 0.6$ (the values are obtained numerically). For $V_{mR} = 6.01$ a sudden change in the amplitude of vibration appears. The amplitude jumps along the curve V_{mR} to the value $a_S = 0.3$ with $\Omega_S = 0.6$. The further decrease

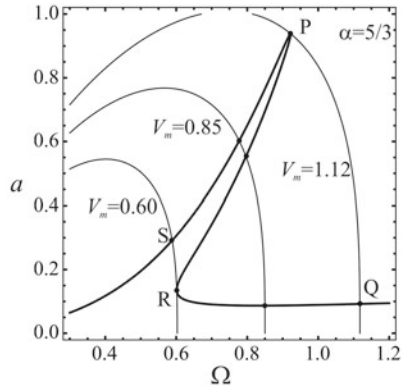

Fig. 3.10 Frequency-response steady state curve obtained analytically for $\alpha = 5/3$ and $C_m = 1$ with characteristic points

of the control parameter V_m produces amplitude and frequency decrease. The region in the $a - \Omega$ plane bounded with the part SP and RQ of the $a - \Omega$ curves and also RS and PQ parts of the $V_m - \Omega$ curves represent the hysteresis and the jump from P to Q and R to S in the system is the so called Sommerfeld effect well known in the non-ideal mechanical systems.

In Fig. 3.9 the values obtained numerically by solving of the original differential equations of motion (3.48) for increasing of the control parameter V_m is plotted with circles (o) and for decreasing of the control parameter with a filled squares (■). Comparing the analytically obtained solutions (full line) with the numerically obtained values it can be seen that the results are in a good agreement.

In Figs. 3.10 and 3.11 the frequency-response curve for the oscillator with order of nonlinearity $\alpha = 2/3$ and motor parameter $C_m = 1$ is plotted. The curves in Fig. 3.10 are obtained by solving the approximate relations (3.72) and (3.147), while in Fig. 3.11 numerically solved differential equations (3.48) are plotted. Both figures show that for slow increasing of Ω and variation of the motor parameter V_m, the amplitude of vibration increases up to the point P whose properties are $a_P = 0.9$, $\Omega_P = 0.9$ and $V_{mP} = 1.12$.

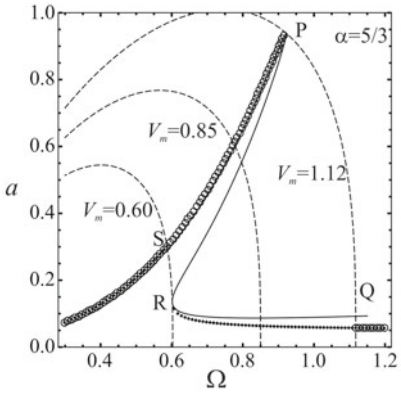

Fig. 3.11 Frequency-response curves for $\alpha = 5/3$ and $C_m = 1$ obtained analytically (*full line*) and numerically (*circles* - for the increasing of V_m, *squares* - for decreasing of V_m)

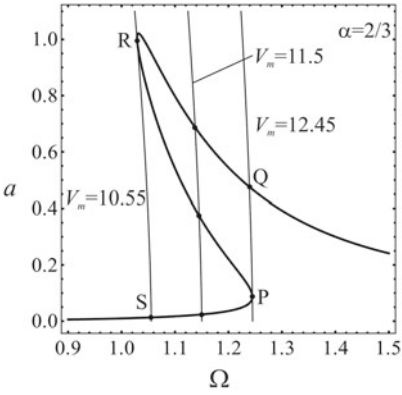

Fig. 3.12 Frequency-response steady state curve obtained analytically for $\alpha = 2/3$ and $C_m = 10$ with characteristic points

Along the curve V_{mP} the jump phenomena from P to Q ($a_Q = 0.055, \Omega_Q = 1.115$) occurs: the frequency Ω_Q is higher than Ω_P, and the amplitude a_Q is smaller than a_P. During further increase of the control parameter V_m, the amplitude of vibration decreases while the frequency Ω increases. If the value of the control parameter V_m is decreased, the steady-state locus in $a - \Omega$ plane moves to left along the $a - \Omega$ curve to the point R. The frequency decreases to $\Omega_R = 0.6$ and the amplitude increases to $a_R = 0.125$ when $V_{mR} = 0.6$. Then a sudden change in the amplitude of vibration appears. The amplitude jumps along the curve V_{mR} to the amplitude $a_S = 0.3$ and frequency $\Omega_S = 0.585$. The further decrease of the control parameter V_m produces amplitude and frequency decrease. The bounded region SPQR represents the hysteresis plane. Comparing Figs. 3.8 and 3.10 it is seen that the Sommerfeld effect occurs for lower values of the motor parameter V_m if $C_m = 1$ than if it is $C_m = 10$.

In Fig. 3.11 the numerically obtained $a - \Omega$ diagrams are plotted: V_m is increased (o), and V_m is decreased (■). These numerically obtained results by solving (3.48) are compared with analytically obtained results (full line curves). The difference between the analytical and numerical solutions is negligible.

In Figs. 3.12 and 3.13 the analytically and numerically obtained amplitude - frequency curves for the oscillator with the order of nonlinearity $\alpha = 2/3$ and motor parameter $C_m = 10$ are plotted. The analytical solutions are obtained by solving (3.72) and (3.147), and the numerical solutions by solving (3.48). The computation procedure was the same to that made in the previous calculation.

First, the control parameter V_m was slowly increased. The steady-state frequency and amplitude increase, too, up to P, when the control parameter has the value $V_{mP} = 12.45$ and the amplitude and frequency are $a_P = 0.075$, $\Omega_P = 1.24$. These values are obtained analytically by solving the relations (3.149)–(3.151). For that value of control parameter ($V_{mP} = 12.45$) a sudden change in amplitude occurs for the almost

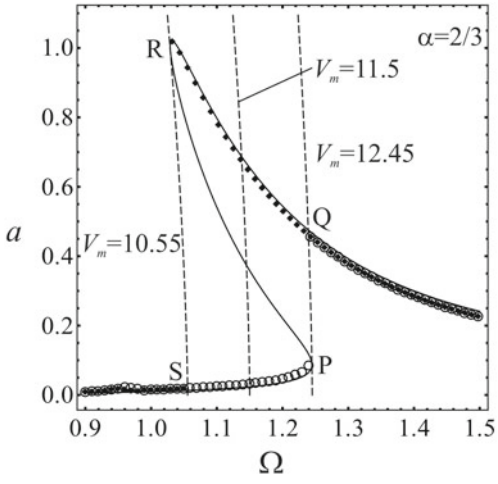

Fig. 3.13 Frequency-response curves for $\alpha = 2/3$ and $C_m = 10$ obtained analytically (*full line*), numerically (*circles* - for the increasing of V_m, *squares* - for decreasing of V_m)

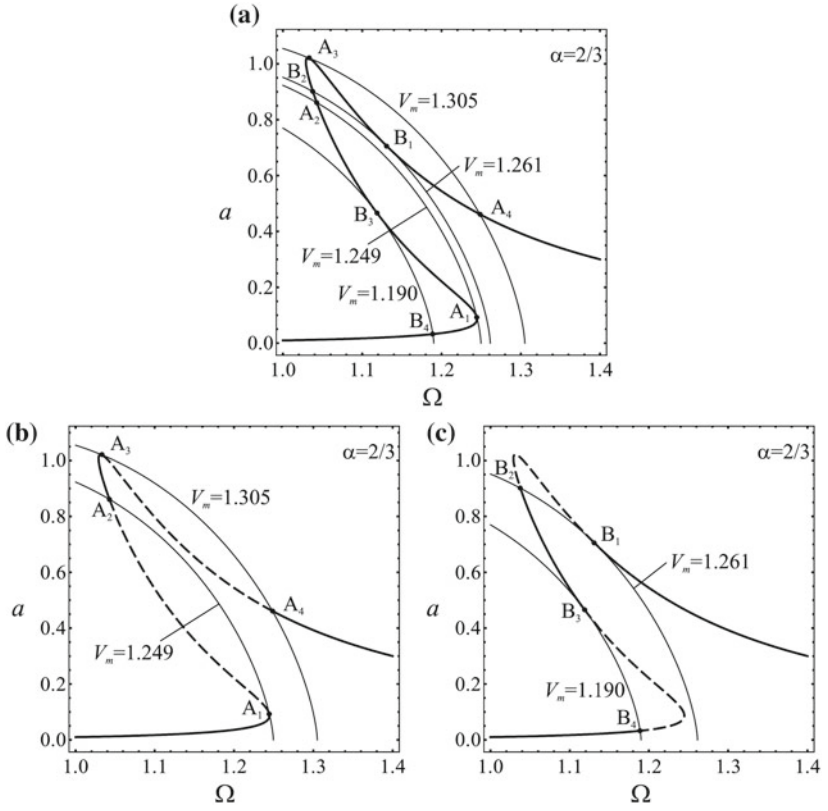

Fig. 3.14 Frequency-response steady state curve obtained analytically for $\alpha = 2/3$ and $C_m = 1$: **a** with characteristic points, **b** for increasing of V_m, **c** for decreasing of V_m

the same frequency. Namely, there is the jump to the point Q with the following values of the amplitude and frequency: $a_Q = 0.475$, $\Omega_Q = 1.22$. Increasing the value of V_m gives decreasing of the amplitude a and increasing of Ω. If the control parameter is V_m and the frequency Ω are decreased, the amplitude of vibration increases up to $a_R = 1.0$ for $V_{mR} = 10.55$ and $\Omega_R = 1.03$. At that value of the control parameter the jump to another steady state position occurs with amplitude $a_S = 0.02$ and frequency $\Omega_S = 1.04$. Further decrease of the control parameter gives also the decrease of the amplitude and frequency. Finally, it can be concluded that the Sommerfeld effect and the jump phenomena occur for $V_{mP} = 12.45$ and $V_{mR} = 10.55$.

Comparing the analytically obtained curve (full line) and the numerically obtained curves for the case when the control parameter increases (o) and when it decreases (■) it can be seen that the difference is negligible (see Fig. 3.13).

In Figs. 3.14 and 3.15 the frequency-response curve for the oscillator with order of nonlinearity $\alpha = 2/3$ and motor parameter $C_m = 1$ is plotted. The curves in Fig. 3.14 are obtained by solving the approximate relations (3.72) and (3.147), while

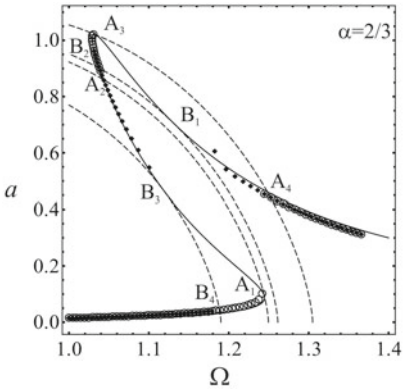

Fig. 3.15 Frequency-response curves for $\alpha = 2/3$ and $C_m = 1$ obtained analytically (*full line*) and numerically (*circles* - for the increasing of V_m, *squares* - for decreasing of V_m)

in Fig. 3.15 numerically solved differential equations (3.48) are plotted. In Fig. 3.14b the steady-state motion for increasing value of the control parameter V_m is plotted. The amplitude of vibration increases slowly with the frequency up to the point A_1 with coordinates $a_{A1} = 0.1, \Omega_{A1} = 1.24$ for the control parameter $V_{mA1} = 1.249$. For that value of the control parameter the other steady state motion is with the amplitude $a_{A2} = 0.875$, and frequency $\Omega_{A2} = 1.04$. For this value of the control parameter the amplitude increases significantly, and the frequency decreases. For higher values of the control parameter the tendency of increase but also decreasing of the frequency is evident. For the control parameter $V_{mA3} = 1.305$ the peak amplitude $a_{A3} = 1.025$ for $\Omega_{A3} = 1.03$ is reached. For this value of control parameter the another steady state motion is with amplitude and frequency $a_{A4} = 0.455, \Omega_{A4} = 1.25$, respectively. Further increase of the control parameter V_m gives the decrease of the amplitude and increase of the frequency.

In Fig. 3.14c the procedure is repeated but in the opposite direction: the control parameter V_m is decreased. Decreasing V_m, the amplitude is increasing up to $a_{B1} = 0.7$and the frequency is decreased to $\Omega_{B1} = 1.13$ for $V_{mB1} = 1.261$. At that value of the control parameter a jump to the amplitude $a_{B2} = 0.9$ and frequency $\Omega_{B2} = 1.04$ occurs. Further decrease of the control parameter causes decrease of the amplitude but increase of the frequency to the boundary values $a_{B3} = 0.475$, $\Omega_{B3} = 1.12$ for $V_{mB3} = 1.190$. For that value of control parameter the other steady state motion is with parameters $a_{B4} = 0.025$, $\Omega_{B4} = 1.19$. Decreasing V_m the amplitude and frequency decrease. In Fig. 3.14a the four values of the control parameter V_m for with the amplitude - frequency curve of the motor is the tangent of the steady state curve are shown. It means, that for Ω slowly increased two times the jump phenomena appear: from A_1 to A_2 (the amplitude jumps to a higher value) and from A_3 to A_4 (the amplitude jumps to a smaller value) as is shown in Fig. 3.14b. For slow decreasing of Ω the amplitude jumps two times in the steady-state curve, too (see Fig. 3.14c) from B_1 to B_2 (the amplitude jumps to a higher value) and from B_3 to B_4 (the amplitude jumps to a smaller value).

In Fig. 3.15 the numerically obtained $a - \Omega$ diagrams are plotted: V_m is increased (o), and V_m is decreased (■). These numerically obtained results by solving (3.48) are compared with analytically obtained results (full line curves). The difference between the analytical and numerical solutions is negligible.

In Fig. 3.16 the influence of the control parameter V_m on amplitude-frequency curve obtained analytically by solving (3.72) and (3.147) for the linear oscillator $\alpha = 1$ and motor parameter $C_m = 1$ is analyzed. In the diagram two values of the control parameter for which the Sommerfeld effect occurs is obtained. For the case of increasing frequency, the control parameter for which two steady state motions P($a_P = 1$, $\Omega_P = 1$) and Q($a_Q = 0.14$, $\Omega_Q = 1.24$) exist is $V_{mP} = 1.251$. For the case of decreasing frequency, for the control parameter $V_{mR} = 1.101$ the jump is from R($a_R = 425$, $\Omega_R = 1.06$) to S($a_S = 0.075$, $\Omega_S = 0.7$).

In Fig. 3.17 we plot the case where the Sommerfeld effect is suppressed. The parameters of the system are $\alpha = 2/3$, $\varepsilon = 0.1$, $\mu_1 = 0.5$, $\eta_1 = 0.5$, $p^2 = 1$ and $\zeta_1 = 1.2$. Two values of C_m are considered: $C_m = 0.85$ (Fig. 3.17a) and $C_m = 5$ (Fig. 3.17b) while V_m is varied. The first value for C_m is computed according to (3.158) and the second value is an arbitrary one. It can be seen that for $C_m = 5$ the V_m intersects the A-Ω curve in one, two or three points giving the Sommerfeld effect.

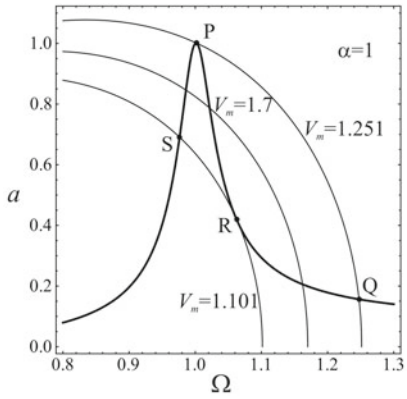

Fig. 3.16 Frequency-response steady state curve obtained analytically for $\alpha = 1$ and $C_m = 1$ with characteristic points

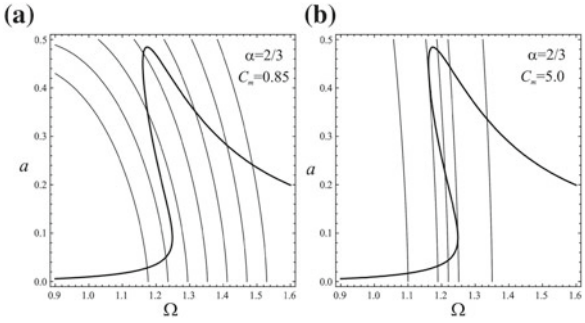

Fig. 3.17 Frequency-response steady state curve obtained analytically for $\alpha = 2/3$ and: **a** $C_m = 0.85$, and **b** $C_m = 5$

For $C_m = 0.85$ only one intersection point of V_m with the amplitude frequency exists and no amplitude jump exists. Thus, the Sommerfeld effect is eliminated.

Comparing the curves and the results plotted in Figs. 3.8, 3.9, 3.10, 3.11, 3.12, 3.13, 3.14, 3.15 and 3.16 the following is concluded:

1. The amplitude-frequency curve bends on right for $\alpha > 1$ (Figs. 3.8 and 3.9), on the left for $\alpha < 1$ (Figs. 3.12, 3.13, 3.14 and 3.15) and is straight for $\alpha = 1$ (Fig. 3.16).
2. For $C_m = 10$ the lines for V_m curves in Figs. 3.8, 3.9, 3.12 and 3.13 are closed to the vertical direction and this case is close to the ideal system. For the ideal system, the oscillator has no influence on the motion of the motor and there is no coupling between these two motions. The ideal system has one-degree-of-freedom and the motion of the oscillator is forced with a time periodical excitation force. The mathematical model of the system is a second order differential equation. For $C_m = 10$ (see Figs. 3.14, 3.15 and 3.16) the V_m curves are bent and the properties of non-ideal system are highly significant. For $C_m = 1$ and $\alpha = 1$ two characteristic values of the control parameter V_m are evident (see Fig. 3.16), while for $C_m = 10$ and $\alpha = 2/3$ even four (Figs. 3.14 and 3.15).
3. In the system with order of nonlinearity $\alpha = 2/3$ the Sommerfeld effect can be eliminated by suitable assumption of the value of the parameter C_m (see Fig. 3.17). Namely, for $C_m = 5$ the effect of jump occurs (Fig. 3.14b), while for the critical value $C_m = 0.85$ and any value of V_m, the Sommerfeld effect is eliminated.

3.3.6 Conclusion

Analyzing the results the following is concluded:

1. In the non-ideal system which contains a pure nonlinear oscillator (order of the nonlinearity is integer or non-integer) and a motor with linear torque properties (a non-ideal source) for certain parameter values the resonant phenomena appears.
2. The approximate averaging procedure, based on the introduction of additional slow variables, as it is assumed that the angular velocity and the frequency of the structure are functions of these variables, is appropriate for analytical analysis of the problem. The suggested averaging procedure gives the equations which are suitable for analysis of the near resonant case. Results which are obtained are applicable for the analysis of the characteristic properties of the system:

   (a) The amplitude-frequency curve bends on right for the nonlinearity of the order higher than 1, i.e., the order is a positive rational number higher than 1. The amplitude-frequency curve bends on the left, if the nonlinearity is a positive rational number smaller than 1. For the linear case,the backbone curve of the amplitude-frequency steady state curve is straight.
   (b) The approximate value of the control parameter for the non-ideal source is analytically calculated applying the method of equating the gradient of the both amplitude-frequency curves (of the oscillator and of the motor) in

the intersection points. The criteria for the Sommerfeld effect is analytically obtained.

(c) The Sommerfeld effect occurs not only for the linear case and when the nonlinearity is higher than 1 (as it is previously published), but also if the nonlinearity is a positive rational number smaller than 1.

(d) The parameters of the energy source effect the steady-state properties of the non-ideal mechanical system. The both parameters of the motor torque ($V_{m\phi}$ and $C_{m\phi}$) and also their rate determine the motion properties. Hence, independently on the order of nonlinearity, the higher the value of $C_{m\phi}$ the system tends to the ideal one.

(e) For the case when the nonlinearity is of the order smaller than 1, the amplitude jump effect may occur two times during increase of the motor property $V_{m\phi}$ and two times during its decrease. For certain motor property the characteristic curve may be the tangent of the amplitude-frequency curve in two points during increase of $V_{m\phi}$ and also during its decrease, and for these values the jump effect occur. In the linear non-ideal oscillator and in the oscillator with a nonlinearity higher than 1 the jump phenomena is evident once during increasing and once during decreasing of $V_{m\phi}$. Namely, the characteristic of the motor is the tangent of the amplitude-frequency curve for one $V_{m\phi}$ during increase, and for other value during decrease.

4. The method given in this text obtains motor torque parameters which can suppress the Sommerfeld effect in the non-ideal mechanical system with the positive nonlinearity of order smaller than 1. The Sommerfeld effect and the jump phenomena in the amplitude for non-ideal system may be suppressed by these critical parameter values.
5. Comparing the analytical and numerical solutions it is evident that they are in a good agreement independently on the order of nonlinearity.

3.4 Stable Duffing Oscillator and a Non-ideal Energy Source

Let us consider a motor operating on a structure with strong cubic nonlinearity (Fig. 3.18). Oscillator is of Duffing type and is connected with the motor with limited power supply. The motor has an eccentric mass which is the part of the non-ideal perturbation source. The driving of the system comes from the unbalanced rotor linked to the oscillator fed by an electric motor. The driven system is taken as a consequence of the dynamics of the whole system (oscillator plus rotor). Duffing oscillator, connected with non-ideal energy source, is of hardening type with strong cubic nonlinearity which was widely investigated by Krylov and Bogolubov (1943), Ueda (1985), Fang and Dowell (1987), Pezeshki and Dowell (1988), Yuste and Bejarano (1986, 1990), Cheng et al. (1991), Chen and Cheung (1996), Chen et al. (1998), Gendelman and Vakakis (2000), Mickens (2001, 2006), Andrianov (2002),

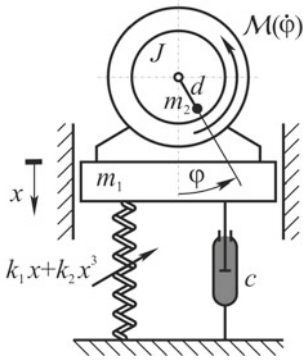

Fig. 3.18 Model of the motor-structure non-ideal system

He (2002), Hu and Xiong (2003), Andrianov and Awrejcewicz (2003a, b), Amore and Aranda (2005), Cveticanin (2004, 2006, 2011), Ozis and Yildirm (2007), Belendez et al. (2007), Cveticanin et al. (2010), Kovacic et al. (2010) and others. The structure of mass M is connected to a fixed basement by a non-linear spring and a linear viscous damper (damping coefficient c). The nonlinear spring stiffness is given by $k_1x + k_2x^3$, where x denotes the structure displacement with respect to some equilibrium position in the absolute reference frame. The motion of the structure is due to an in-board non-ideal motor driving an unbalanced rotor. We denote by φ the angular displacement of the rotor unbalance, and model it as a particle of mass m and radial distance d from the rotating axis. The moment of inertia of the rotating part is J. For the resonant case the structure has an influence on the motor input or output. The forcing function is dependent of the system it acts on and the source is of non-ideal type.

The non-ideal problem has two - degrees of freedom, represented by the generalized coordinates x and φ. The kinetic energy T, potential energy U and the dissipative function Φ are expressed by

$$T = \frac{1}{2}M\dot{x}^2 + \frac{1}{2}m(\dot{x}^2 + d^2\dot{\varphi}^2 - 2d\dot{x}\dot{\varphi}\sin\varphi) + \frac{1}{2}J\dot{\varphi}^2, \tag{3.159}$$

$$U = \frac{1}{2}k_1x^2 + \frac{1}{4}k_2x^4 - (M+m)gx - mgd\cos\varphi, \qquad \Phi = \frac{1}{2}c\dot{x}^2. \tag{3.160}$$

A dot denotes differentiation with respect to time t. Lagrange's equations of motion for the system are in general

$$\frac{d}{dt}\left(\frac{\partial T}{\partial \dot{x}}\right) - \frac{\partial T}{\partial x} + \frac{\partial U}{\partial x} + \frac{\partial \Phi}{\partial \dot{x}} = Q_x,$$
$$\frac{d}{dt}\left(\frac{\partial T}{\partial \dot{\varphi}}\right) - \frac{\partial T}{\partial \varphi} + \frac{\partial U}{\partial \varphi} + \frac{\partial \Phi}{\partial \dot{\varphi}} = Q_{\dot{\varphi}},$$

where Q_x and $Q_{\dot{\varphi}}$ are generalized forces.

The differential equations of motion have the form

$$\ddot{x}(M+m)+c\dot{x}-md(\ddot{\varphi}\sin\varphi+\dot{\varphi}^2\cos\varphi)+k_1x+k_2x^3=(M+m)g,$$
$$(J+md^2)\ddot{\varphi}-md\ddot{x}\sin\varphi+mgd\sin\varphi=\mathcal{M}(\dot{\varphi}), \quad (3.161)$$

where $\mathcal{M}(\dot{\varphi})$ is the motor torque. The most often used model of the torque is the linear moment-speed relation (see Dimentberg et al. 1997)

$$\mathcal{M}(\dot{\varphi})=M_0\left(1-\frac{\dot{\varphi}}{\Omega}\right), \quad (3.162)$$

where M_0 and Ω are constant values.

It is convenient to normalize the coordinates and time according to

$$x\longrightarrow y=\frac{\Omega^2}{g}x, \qquad t\longrightarrow\tau=\Omega t, \quad (3.163)$$

where g is the gravity constant. By introducing (3.163) the differential equations (3.161) transform into

$$y''+\zeta y'+p^2y+\gamma y^3=1+\mu(\varphi''\sin\varphi+\varphi'^2\cos\varphi),$$
$$\varphi''=\eta y''\sin\varphi-\eta\sin\varphi+F(1-\varphi'), \quad (3.164)$$

where

$$p=\frac{\omega^*}{\Omega}, \qquad \omega^{*2}=\frac{k_1}{M+m}, \qquad \gamma=\frac{k_3g^2}{(M+m)\Omega^6}, \qquad \zeta=\frac{c}{\Omega(M+m)},$$
$$\mu=\frac{m}{M+m}\frac{d\Omega^2}{g}, \qquad \eta=\frac{gmd}{\Omega^2(J+md^2)}, \qquad F=\frac{M_0}{\Omega^2(J+md^2)}, \quad (3.165)$$

and prime denotes differentiation with respect to τ. The differential equations (3.164) are non-linear and coupled.

3.4.1 Asymptotic Solving Method

In the regime near resonant the difference between the excitation frequency is close to the natural frequency. For the near resonant case one can write

$$\varphi'-p=\varepsilon\sigma, \quad (3.166)$$

where $\varepsilon\sigma$ is the detuning parameter with the small parameter $\varepsilon << 1$. Expressing parameters of equations (3.165) by

$$\zeta=\varepsilon\zeta_1, \qquad \gamma=\varepsilon\gamma_1, \qquad \mu=\varepsilon\mu_1, \qquad \eta=\varepsilon\eta_1, \qquad F=\varepsilon F_1, \quad (3.167)$$

the differential equations of motions have the form

$$z'' + p^2 z = \varepsilon\mu_1 \left(\varphi'' \sin\varphi + \varphi'^2 \cos\varphi\right) - \varepsilon\zeta_1 z' - \varepsilon\gamma_1 \left(z + \frac{1}{p^2}\right)^3\Bigg],$$
$$\varphi'' = \varepsilon\eta_1 z'' \sin\varphi - \varepsilon\eta_1 \sin\varphi + \varepsilon F_1(1 - \varphi'), \tag{3.168}$$

where the new variable is

$$z = y - \frac{1}{p^2}. \tag{3.169}$$

Expressing z" and φ" from the Eq. (3.168) and assuming only the terms to $O(\varepsilon^2)$ we obtain

$$z" + p^2 z = \varepsilon\left[\mu_1 \varphi'^2 \cos\varphi - \zeta_1 z' - \gamma_1 (z + \frac{1}{p})^3\right] + \varepsilon^2 \ldots,$$
$$\varphi" = \varepsilon\left[F_1(1 - \varphi') - \eta_1(1 + p^2 z)\sin\varphi\right] + \varepsilon^2 \ldots. \tag{3.170}$$

Following the reference (Warminski et al. 2001)

$$z = a\cos(\varphi + \psi), \tag{3.171}$$

where a and ψ are the new coordinates. The first derivative is

$$z' = -ap\sin(\varphi + \psi), \tag{3.172}$$

when

$$a'\cos(\varphi + \psi) - a(\omega + \psi' - p)\sin(\varphi + \psi) = 0. \tag{3.173}$$

Determining the second derivative of z and substituting (3.171) and (3.172) into (3.170) we obtain

$$-a' p \sin(\varphi + \psi) - ap(\omega + \psi')\cos(\varphi + \psi) + p^2 a\cos(\varphi + \psi)$$
$$= \varepsilon\mu_1\omega^2\cos\varphi + ap\varepsilon\zeta_1 \sin(\varphi + \psi) - \varepsilon\gamma_1\left[a\cos(\varphi + \psi) + \frac{1}{p}\right]^3,$$
$$\omega' = \varepsilon F_1(1 - \omega) - \varepsilon\eta_1[1 + ap^2\cos(\varphi + \psi)]\sin\varphi. \tag{3.174}$$

Equations (3.173) and (3.174) lead to the derivatives a', ψ', φ' and ω'

$$a' = -\sin(\varphi + \psi)\left\{\frac{\varepsilon\mu_1}{p}\omega^2\cos\varphi + a\varepsilon\zeta_1\sin(\varphi + \psi)\right.$$
$$\left. -\frac{1}{p}\varepsilon\gamma_1\left[a\cos(\varphi + \psi) + \frac{1}{p}\right]^3\right\},$$

$$a\psi' = \varepsilon\sigma a - \cos(\varphi+\psi)\left\{\frac{\varepsilon\mu_1}{p}\omega^2\cos\varphi + a\varepsilon\zeta_1\sin(\varphi+\psi) - \frac{1}{p}\varepsilon\gamma_1\left[a\cos(\varphi+\psi)+\frac{1}{p}\right]^3\right\},$$
$$\omega' = \varepsilon F_1(1-\omega) - \varepsilon\eta_1[1+ap^2\cos(\varphi+\psi)]\sin\varphi, \qquad \varphi' = \omega. \quad (3.175)$$

Unfortunately, the closed form analytical solution for (3.175) is complicate to be obtained and the numerical methods are convenient.

3.4.2 *Stability of the Steady State Solution and Sommerfeld Effect*

Introducing the averaging procedure (see Bogolyubov and Mitropolskij 1974)

$$a' = \frac{\varepsilon}{2\pi}\int_0^{2\pi} f_a d\varphi, \qquad a\psi' = \frac{\varepsilon}{2\pi}\int_0^{2\pi} f_\psi d\varphi, \qquad \omega' = \int_0^{2\pi} f_\omega d\varphi, \quad (3.176)$$

where

$$f_a = -\frac{1}{p}\sin(\varphi+\psi)\left\{\mu_1\omega^2\cos\varphi + ap\zeta_1\sin(\varphi+\psi) - \gamma_1\left[a\cos(\varphi+\psi)+\frac{1}{p}\right]^3\right\},$$
$$f_\psi = a\sigma - \frac{1}{p}\cos(\varphi+\psi)\{\mu_1\omega^2\cos\varphi + ap\zeta_1\sin(\varphi+\psi) - \gamma_1\left[a\cos(\varphi+\psi)+\frac{1}{p}\right]^3\right\},$$
$$f_\omega = F_1(1-\omega) - \eta_1[1+ap^2\cos(\varphi+\psi)]\sin\varphi, \quad (3.177)$$

the differential equations (3.175) are transformed into

$$\omega' = \varepsilon\left[F_1(1-\omega) + \frac{1}{2}\eta_1 ap^2\sin\psi\right],$$
$$a' = -\frac{\varepsilon}{2}\left(a\zeta_1 + \frac{\mu_1\omega^2}{p}\sin\psi\right),$$
$$\psi' = \varepsilon\sigma - \frac{\varepsilon}{2p}\left(\frac{\mu_1\omega^2}{a}\cos\psi - \frac{3\gamma_1 a^2}{4} - \frac{3\gamma_1}{p^2}\right). \quad (3.178)$$

For the steady-state response, Eq. (3.178) have the form

$$
\begin{aligned}
F_1(1-\omega_S)+\frac{1}{2}\eta_1 a_S p^2 \sin\psi_S &= 0,\\
a_S+\frac{\mu_1\omega_S^2}{p}\sin\psi_S &= 0,\\
\sigma-\frac{1}{2p}\left(\frac{\mu_1\omega_S^2}{a_S}\cos\psi_S-\frac{3\gamma_1 a_S^2}{4}-\frac{3\gamma_1}{p^2}\right) &= 0,
\end{aligned}
\tag{3.179}
$$

where S denotes the steady state values. Combining the second and the third Eq. (3.179) we obtain

$$
a_S^2\left\{\frac{\zeta_1^2}{4}+\left[\sigma+\frac{3\gamma_1}{2p}\left(\frac{a_S^2}{4}+\frac{1}{p^2}\right)\right]^2\right\}=\left(\frac{\mu_1\omega_S^2}{2p}\right)^2, \tag{3.180}
$$

while combining the first and the second Eq. (3.179) yields

$$
F_1\mu_1\omega_S^2(1-\omega_S)=\frac{1}{2}\zeta_1\eta_1 a_S^2 p^3. \tag{3.181}
$$

Expressing a_S in (3.181) and substituting into (3.180) the $\omega_S(F_1)$ function is obtained

$$
8F_1(1-\omega_S)\left\{\frac{\zeta_1^2}{4}+\left[\omega_S-p+\frac{3\gamma_1}{2p^5}\left(\frac{\mu_1\omega_S^2F_1(1-\omega_S)}{2\zeta_1\eta_1 p}+1\right)\right]^2\right\}-\mu_1\zeta_1\eta_1 p\omega_S^2=0. \tag{3.182}
$$

The number of real solution is one, two or three and it depends on the control parameter F_1. To determine which of the solutions actually correspond to a realizable motion, we need to consider the stability of the solutions. We determine the stability by determining the nature of the singular points of (3.179). To accomplish this, we let

$$
a=a_S+a_1, \qquad \psi=\psi_S+\psi_1, \qquad \omega=\omega_S+\omega_1. \tag{3.183}
$$

Substituting (3.183) into (3.179) and neglecting all but the linear terms in a_1, ψ_1, ω_1 we obtain

$$
\begin{aligned}
\omega_1' &= \varepsilon\left[-F_1\omega_1+\frac{1}{2}\eta_1 a_1 p^2\sin\psi_S+\frac{\psi_1}{2}\eta_1 a_S p^2\cos\psi_S\right],\\
a_1' &= -\frac{\varepsilon}{2}\left(a_1\zeta_1+\psi_1\frac{\mu_1\omega_S^2}{p}\cos\psi_S+2\frac{\mu_1\omega_S\omega_1}{p}\sin\psi_S\right),\\
\psi_1' &= -\omega_1-\frac{\varepsilon}{2p}\left(2\frac{\mu_1\omega_S\omega_1}{a_S}\cos\psi_S-a_1\frac{\mu_1\omega_S^2}{a_S^2}\cos\psi_S\right.\\
&\quad \left.-\psi_1\frac{\mu_1\omega_S^2}{a_S}\sin\psi_S-\frac{3\gamma_1 a_S a_1}{2}\right).
\end{aligned}
\tag{3.184}
$$

Equations (3.184) are linear and have the solution in the form

$$(a_1, \psi_1, \omega_1) = (a_{10}, \psi_{10}, \omega_{10}) \exp(\lambda\tau),$$

where λ is an eigenvalue of the coefficient of matrix. The solutions are stable and hence corresponding motions reliable, if the real part of each eigenvalue is negative or zero.

For the parameter values

$$\varepsilon = 0.1, \quad \zeta_1 = 0.2, \quad \gamma_1 = 0.1, \quad \eta_1 = 1.0, \quad \mu_1 = 0.5, \tag{3.185}$$

using the relations (3.180) and (3.181), i.e., (3.182) the response-control parameter F_1 and the frequency of vibration-control parameter F_1 diagrams are plotted (Fig. 3.19).

In Fig. 3.20 the frequency-response curves obtained numerically and analytically by solving the Eqs. (3.180) and (3.181) are plotted. Comparing the solutions it can be concluded that the difference between "exact" numerical solution and approximate analytical solution is negligible. Analyzing the obtained curves and the relation (3.181) it is evident that the curve depends on the control parameter F_1. For $\omega_S = 2/3$ the maximal response

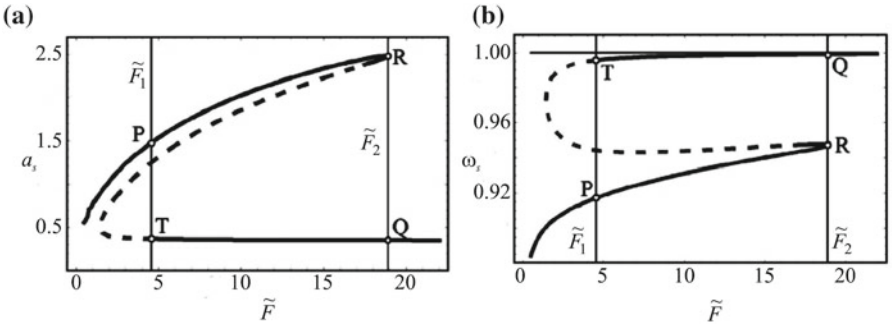

Fig. 3.19 Jump effect for: **a** amplitude-control parameter curve, **b** frequency-control parameter curve

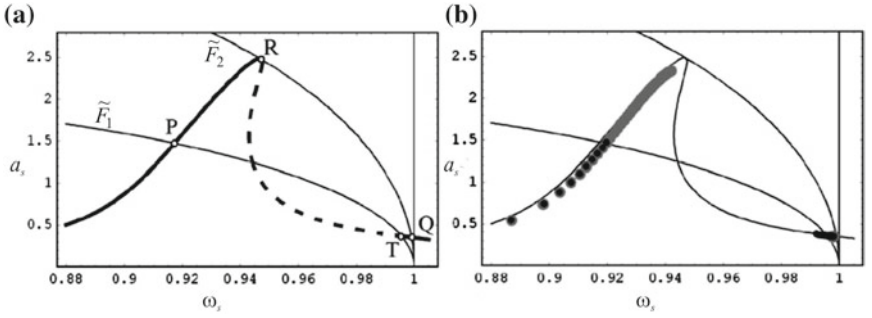

Fig. 3.20 Frequency-response curve obtained: **a** analytically, **b** numerically

$$a_{S\max} = \frac{2}{3p}\sqrt{\frac{2\mu_1}{3\zeta_1\eta_1 p}F_1},$$

is a function of F_1, but is not dependent on the parameter of non-linearity γ_1.

Figures 3.19 and 3.20 show the characteristic points in the diagrams: point R and point T. Between these points the solution is unstable while all those outside this region are stable. Point R is the peak in $a_S - \omega_S$, $a_S - F_1$ and $F_1 - \omega_S$ diagrams. Analyzing the relation (3.182) and equating the first derivative to zero ($dF_1/d\omega_S = 0$)

$$\begin{aligned} 0 = -8F_1 &\left\{\frac{\zeta_1^2}{4} + \left[\omega_S - p + \frac{3\gamma_1}{2p^5}\left(\frac{\mu_1\omega_S^2 F_1(1-\omega_S)}{2\zeta_1\eta_1 p} + 1\right)\right]^2\right\} \\ &+2F_1(1-\omega_S)\left[\omega_S - p + \frac{3\gamma_1}{2p^5}\left(\frac{\mu_1\omega_S^2 F_1(1-\omega_S)}{2\zeta_1\eta_1 p} + 1\right)\right] \\ &\left[1 + \frac{3\gamma_1}{2p^5}\frac{\mu_1 F_1(2\omega_S - 3\omega_S^2)}{2\zeta_1\eta_1 p}\right] - 2\mu_1\zeta_1\eta_1 p\omega_S. \end{aligned}$$

the peak is obtained. The locus of the peak (point R) is according to (3.180)

$$\omega_{SR} = p - \frac{3\varepsilon\gamma_1}{2p}\left(\frac{a_{SR}^2}{4} + \frac{1}{p^2}\right), \tag{3.186}$$

and the amplitude is $a_{SR} = \mu_1\omega_{SR}^2/\tilde{\alpha}p$. Substituting (3.186) into the relation (3.181) we obtain the value of the control parameter for the peak amplitude

$$F_{1R} = \frac{\eta_1 p\mu_1\omega_{SR}^2}{2\zeta_1(1-\omega_{SR})}. \tag{3.187}$$

Substituting the parameter values (3.185) into (3.187) the numeric value of the control parameter is $F_{1R} = 18.246$. For that calculated value of the control parameter and the known value of the parameter of nonlinearity ($\gamma_1 = 0.1$) the amplitude and frequency of Q are obtained by solving the relations (3.180) and (3.181). For the control parameter $F_{1T} = 4.57$ two stable solutions are obtained: T with a_{ST} and ω_{ST} and P with a_{SP} and ω_{SP}. We note that there are gaps in the diagrams (see Figs. 3.19 and 3.20) where no steady state response exists. The gaps are not the same for increasing and decreasing the control parameter F_1. Increasing the control parameter causes the increase of the amplitude and frequency of vibrations to R. Then the effect of jump to smaller amplitude and higher frequency in Q appears. Decreasing the control parameter ξ_1 decreases the frequency and increases the amplitude to T and then jump into P with higher amplitude and smaller frequency occurs. The same hysteresis is seen in Fig. 3.20. This phenomena of jump is called the Sommerfeld effect in non-ideal systems.

To eliminate the Sommerfeld effect for the certain value of the control parameter F_{1R} the parameter of nonlinearity has to be calculated. The Eq. (3.180) indicates the peak amplitude

$$a_{SR} = \frac{\mu_1}{\zeta_1 p}\omega_{SR}^2. \tag{3.188}$$

The function $a_{SR}(\omega_{SR})$ is independent on the parameter of non-linearity γ_1. The relation (3.181) gives the dependence of amplitude a_S on ω_S for various values of control parameter ξ_1. Using (3.188) and (3.181) we obtain

$$F_{1R}(1-\omega_{SR}) - \frac{1}{2}\eta_1 \frac{\mu_1}{\zeta_1}\omega_{SR}^2 p = 0. \tag{3.189a}$$

ω_{SR} is the solution of (3.189a) for the control parameter F_{1R}. Substituting ω_{SR} into (3.188) the amplitude a_{SR} is calculated. Introducing the so obtained values ω_{SR} and a_{SR} into (3.180) the value of nonlinear parameter γ_{1R} is determined

$$\gamma_{1R} = \frac{8}{3}\frac{p^3}{a_{SR}^2 p^2 + 4}(p - \omega_{SR}). \tag{3.190}$$

For $\gamma_1 < \gamma_{1R}$ only one stable solution exists for the control parameter F_{1R} and the motion is without jump.

In Fig. 3.21 the $a_S - F_1$ curve for two values of parameter of nonlinearity γ_1 is shown. It is seen that for $\gamma_1 = 0.1$ the bending of the curve is smaller than for $\gamma_1 = 0.15$. For $F_{1R} = 42.1$ and $\gamma_{1R} = 0.15$ two real values of amplitude exist and for $\gamma_1 = 0.1$ only one. It can be concluded that for the real system with parameters (3.185) which works with control parameter $F_{1R} = 42.1$ the parameter of non-linearity of the structure has to be $\gamma_1 < 0.15$. Then, the Sommerfeld effect is eliminated.

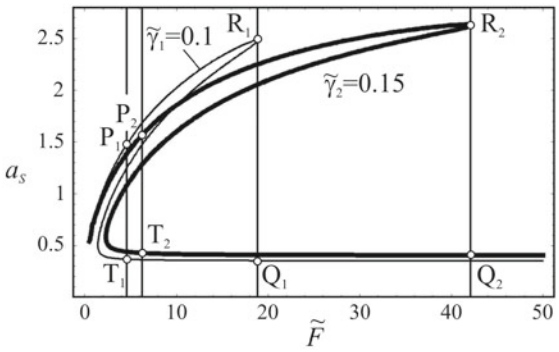

Fig. 3.21 Frequency-control parameter curve for various values of parameter of non-linearity

3.4.3 Numerical Simulation and Chaotic Behavior

To prove the analytically obtained results the numerical experiment is done. The system (3.51) is rewritten in the form

$$\begin{aligned}
y_1' &= y_2,\\
y_2' &= \frac{1}{1-\mu\eta\sin^2 y_3}(-\zeta y_2 - p y_1 - \gamma y_1^3 + 1\\
&\quad +\mu\sin y_3(\mu y_4^2\cos y_3 - \eta\sin y_3 + F(1-y_4))),\\
y_3' &= y_4,\\
y_4' &= \frac{\eta\sin y_3}{1-\mu\eta\sin^2 y_3}(-\zeta y_2 - p y_1 - \gamma y_1^3 + 1 + \mu y_4^2\cos y_3\\
&\quad +\mu\sin y_3\,(-\eta\sin y_3 + F(1-y_4)))\\
&\quad -\eta\sin y_3 + F(1-y_4).
\end{aligned} \tag{3.191}$$

A number of numerical simulations are done for various control parameter F. Applying the Runge–Kutta numerical procedure with the fixed step length the system of four first order differential equations (3.191) is solved. The results are plotted in Fig. 3.22. The phase space of the system has out of four dimensions, but we were chiefly interested in position of the oscillator itself. We also plotted the Poincaré map which represents the surface of section $(y_1(\tau_n),y_2(\tau_n))$. The points $(y_1(\tau_n),y_2(\tau_n))$

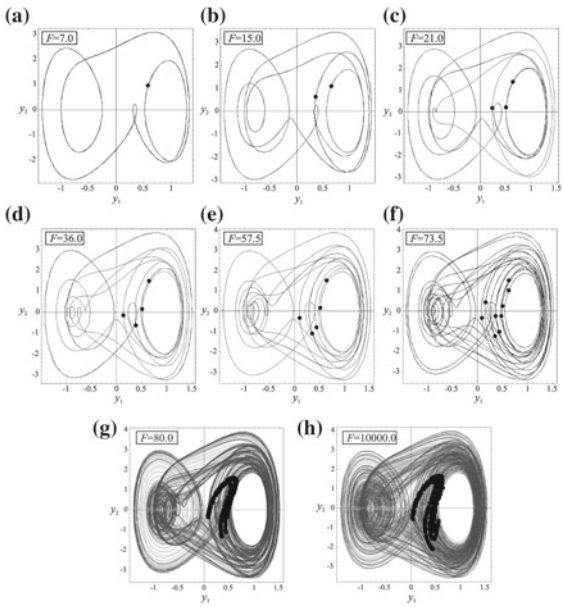

Fig. 3.22 Trajectories in the phase space for various values of the control parameter: **a** periodic solution with period 1, **b** periodic solution with period 2, **c** periodic solution with period 3, **d** periodic solution with period 4, **e** periodic solution with period 5, **f** periodic solution with period 9, **g**, **h** chaotic solution

are captured for $\tau_n = nT$, where $n = 1, 2, \ldots$, with period $T = 2\pi/\bar{\Omega}$. The angular velocity $\overline{\Omega}$ is obtained numerically

$$\overline{\Omega} = \frac{\varphi(\tau_1) - \varphi(0)}{\tau_1} = \frac{y_3(\tau_1) - y_3(0)}{\tau_1}, \tag{3.192}$$

where τ_1 is a long time period for numerical calculation.

For the parameter values of the system, mentioned in the previous section, and the control parameter $F = 7.0$ the trajectory in the phase space and the Poincaré map are plotted (Fig. 3.22a). The motion is periodic with period 1 and frequency $\overline{\Omega} = 0.999$. For $F = 15$ the periodic motion is with period 2 (Fig. 3.22b) and for $F = 21$ with period 3 (Fig. 3.22c). Increasing the value of the control parameter the motion is periodic but the period number increases, too (see Fig. 3.22d–f). For high values of control parameter ($F = 80$ and $F = 10000$) the strange attractor is obtained (Fig. 3.22g, h). The existence of strange attractor signifies chaos which is evident only if the certain criteria for the maximal (local) Lyapunov exponent are satisfied. For computational reasons the vector notation for the system of Eq. (3.191) is introduced

$$Y' = G(Y, P), \tag{3.193}$$

where $Y = [y_1, y_2, y_3, y_4]^T$ is the state space vector, $G = [g_1, g_2, g_3, g_4]$, $P(p, \alpha, \eta, \mu, F)$ is set of parameters and $[...]^T$ is denoting transpose. The equations for small deviations δY from the trajectory $Y(t)$ are

$$\delta Y' = L_{ij}(Y(t))\delta Y, \qquad i, j = 1, 2, \ldots 4, \tag{3.194}$$

where $L_{ij} = \partial g_i / \partial y_j$ is the Jacobian matrix of derivatives

$$\begin{aligned}
&L_{11} = L_{13} = L_{14} = 0, \qquad L_{12} = 1,\\
&L_{21} = -\frac{p + 3\alpha y_1^2}{1 - \mu\eta \sin^2 y_3}, \qquad L_{22} = -\frac{\zeta}{1 - \mu\eta \sin^2 y_3},\\
&L_{23} = \frac{-\mu y_4^2 \sin y_3 + \mu\eta(1 - y_4)\cos y_3}{1 - \mu\eta \sin^2 y_3} - \frac{Q_1}{(1 - \mu\eta \sin^2 y_3)^2},\\
&L_{24} = \frac{2\mu y_4 \cos x_3 - \mu\eta \sin y_3}{1 - \mu\eta \sin^2 y_3}, \quad L_{44} = \frac{\mu\eta y_4 \sin(2y_3) - F}{1 - \mu\eta \sin^2 y_3},\\
&L_{31} = L_{32} = L_{33} = 0, \qquad L_{34} = 1,\\
&L_{41} = -\frac{\eta p \sin y_3 + 3\eta\gamma y_1^2 \sin y_3}{1 - \mu\eta \sin^2 y_3}, \qquad L_{42} = -\frac{\zeta\eta \sin y_3}{1 - \mu\eta \sin^2 y_3},\\
&L_{43} = \frac{\mu\eta y_4^2 \cos(2y_3) - \eta \cos x_3(\zeta y_2 + p y_1 + \gamma y_1^3)}{1 - \mu\eta \sin^2 y_3}\\
&\qquad + \frac{Q_2}{(1 - \mu\eta \sin^2 y_3)^2},
\end{aligned} \tag{3.195}$$

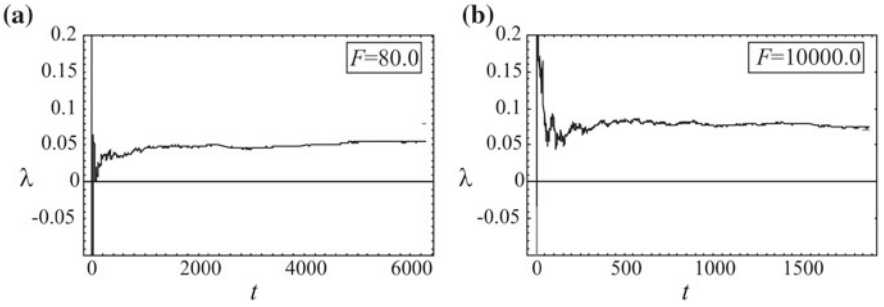

Fig. 3.23 Positive Lyapunov exponent for the control parameters: **a** $F = 80$ and **b** $F = 10000$

where

$$Q_1 = -\mu\eta \sin(2y_3)[\zeta y_2 + py_1 + \gamma y_1^3 - \mu y_4^2 \cos y_3 - \mu F(1 - y_4) \sin y_3],$$
$$Q_2 = \mu\eta \sin(2y_3)[F(1 - y_4) + 0.4\mu\eta y_4^2 \sin(2y_3) - \eta \sin y_3(\zeta y_2 + py_1 + \gamma y_1^3)]. \tag{3.196}$$

The maximal Lyapunov exponent of the system is then as defined by Wolf et al. (1985)

$$\lambda = \lim \frac{1}{t} \log \frac{\|\delta Y(t)\|}{\|\delta Y(0)\|}. \tag{3.197}$$

In Fig. 3.23 we present the local Lyapunov exponent for the control parameters $F = 80$ and $F = 10000$. For the both parameter values the positive Lyapunov exponent is calculated. As it is discussed by Wolf et al. (1985), if the system contains at least one positive Lyapunov exponent the motion is chaotic. The two initially nearby orbits (or trajectories) diverge from each other and the separation of two nearby trajectories increases exponentially with time due to sensitive dependence on initial conditions.

The transition from periodic motion to chaos is by periodic doubling. In Fig. 3.24 the $y_1 - F$ bifurcation diagram is plotted. The bifurcation diagram is obtained for the long time integration of the differential equations (3.191) of the motion. After decay of transient motion a steady state motion is established. The fixed values of the parameters are $\alpha = 0.1$, $\gamma = 9$, $p = 1$, $\mu = 8.373$, $\eta = 0.05$ and the control parameter we choose to work with is F. By increasing parameter F we found sequences of period doubling bifurcations (Fig. 3.24). Diagram starts from $F = 6$ where periodic motion with period $n = 1$ exists. This periodic solution bifurcates on $F \approx 8$ onto period $2T$. Further period doubling bifurcation (period 4, 8, 16,...) leads to chaotic motion for $F \approx 20$. After this interval of chaos the periodic motion with period 3 exists. Further increase of parameter F leads to the new period doubling bifurcation with periods 5, 9, ... and finally to chaos for $F \in [28, 33]$. The next regions of chaotic motion are for $F \in [40, 56]$ and $F > 62$.

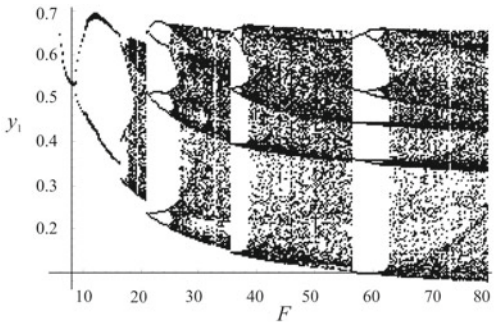

Fig. 3.24 Period doubling bifurcation diagram

Comparing the bifurcation parameter values in Fig. 3.24 with the results of numerical experiment (see Fig. 3.22) it can be concluded that for the control parameter $F = 80$ chaotic motion exists.

3.4.4 Chaos Control

It is of interest to control the chaos in the motion of the system (3.191) and specially of oscillator. There are many methods for chaos control. Dantas and Balthazar (2003) show that if we use an appropriate damping coefficient the chaotic behavior is avoided. The method of Pyragas (1992, 1995) is based on the addition of a special kind of time-continuous perturbation (external force control), which does not change the form of the desired unstable periodic solution, but under certain conditions can stabilize it. The method of Pyragas was applied in the paper. For the external force $\Phi(t)$ the model (3.191) becomes

$$\begin{aligned}
y_1' &= y_2 + \Phi(t),\\
y_2' &= \frac{1}{1-\mu\eta\sin^2 y_3}\{-\zeta y_2 - p y_1 - \gamma y_1^3 + 1 + \mu\sin y_3[\mu y_4^2\cos y_3\\
&\quad -\eta\sin y_3 + F(1-y_4)\},\\
y_3' &= y_4,\\
y_4' &= \frac{\eta\sin y_3}{1-\mu\eta\sin^2 y_3}(-\zeta y_2 - p y_1 - \gamma y_1^3 + 1 + \mu y_4^2\cos y_3\\
&\quad +\mu\sin y_3\,(-\eta\sin y_3 + F(1-y_4))) - \eta\sin y_3 + F(1-y_4). \qquad (3.198)
\end{aligned}$$

The external force $\Phi(t)$ is defined as

$$\Phi(t) = K[y_{up}(t) - y_1(t)], \qquad (3.199)$$

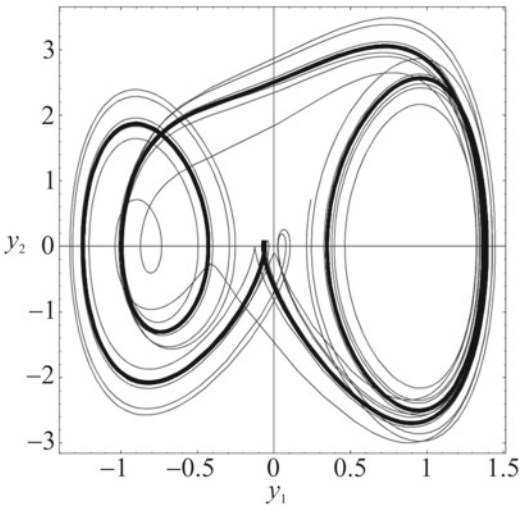

Fig. 3.25 The two-periodic solution: before stabilization (−) and after stabilization (–)

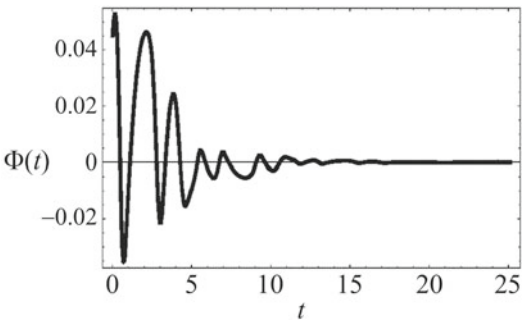

Fig. 3.26 External force-time history diagram

where K is an adjustable weight of the perturbation $\Phi(t)$ and $y_{up}(t)$ is a component of the unstable periodic solution of (3.191) which we wish to stabilize. The function $y_{up}(t)$ is time periodical with period T. For $\Phi(t)$ zero the system has a strange attractor.

However, by selecting the constant K one can achieve the desired stabilization. Using the shooting method suggested by Van Dooren and Janssen (1996) the unstable two periodic unstable solution is detected (Fig. 3.25). Varying the value of the constant K in the interval $[0.1, 2]$ it is concluded that for $K \in [0.3, 2]$ the stabilization is achieved (Fig. 3.25).

For $K = 2$ the function $\Phi(t)$ tends to a very small value (Fig. 3.26) and the component y_1, which is the solution after control, is very close to $y_{up}(t)$.

3.4.5 Conclusion

During passage through resonance of the motor-structure system which is modeled as a stable Duffing oscillator with non-ideal excitation severe vibrations appear. The energy of the system is not used for increasing of the rotation velocity, but is spent for vibrations which are harmful. Very often in the motion of the system near resonance the jump phenomena occurs: at the same value of the control parameter of the motor the amplitude of vibration skips to a higher value with lower frequency or to smaller amplitude with higher frequency. The manifestation depends on the direction of variation of the control setting. The jump phenomena and the increase in power required by a source operating near resonance are manifestations of a non-ideal energy source and are referred to as Sommerfeld effect. The Sommerfeld effect contributes to transform a regular vibration to an irregular chaotic one. It is concluded that in spite of the fact that the structure is modeled as the stable Duffing oscillator chaos appears. In the system the chaos is achieved by period doubling bifurcation. From engineering point of view it is necessary to eliminate the jump effect and the chaotic motion. The elimination of the jump phenomena for the certain control parameter is achieved by using the structure with coefficient of nonlinearity which is smaller than the critical value (3.190). Chaos is controlled using the external force control procedure where the added force does not change the form of the desired unstable periodic solution, but under certain conditions can stabilize it.

Comparing the results obtained applying the approximate analytic methods with those obtained numerically it is concluded that the difference is negligible. It proves the correctness of the used analytic procedure.

3.5 Bistable Duffing Oscillator Coupled with a Non-ideal Source

The model, shown in Fig. 3.27, represents an one degree-of-freedom cart connected to a fixed frame by a nonlinear spring and a dashpot (Warminski et al. 2001). Motion of the cart is due to a non-ideal motor with unbalanced rotor. In the absolute reference frame x denotes the cart displacement and φ denotes the angular displacement of the rotor. Elastic force of the spring is a cubic function of cart position x.

Motion of the system is described with the following equations (Kononenko 1976)

$$\begin{aligned} \ddot{x}(M+m) + c\dot{x} - md(\ddot{\varphi}\sin\varphi + \dot{\varphi}^2\cos\varphi) - k_1 x + k_2 x^3 = 0, \\ (J + md^2)\ddot{\varphi} - md\ddot{x}\sin\varphi = \mathcal{M}(\dot{\varphi}), \end{aligned} \quad (3.200)$$

where $\mathcal{M}(\dot{\varphi})$ is the motor torque. For further consideration, let us introduce the dimensionless length and dimensionless time

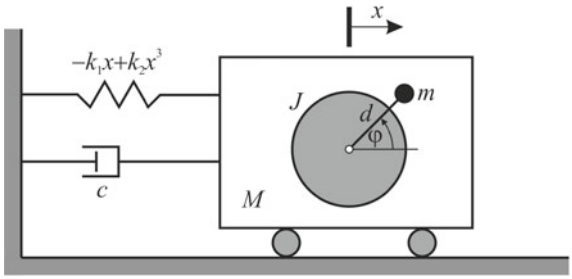

Fig. 3.27 Model of the system

$$y = \frac{x}{d}, \quad \tau = \omega t, \tag{3.201}$$

where d is the distance of the unbalanced mass to the shaft center and

$$\omega = \sqrt{\frac{k_1}{m+M}}. \tag{3.202}$$

Using (3.201) and (3.202), the dimensionless equations of motion are

$$\begin{aligned} y'' + \zeta y' - y + \gamma y^3 &= \frac{m}{M+m}(\varphi'' \sin\varphi + \varphi'^2 \cos\varphi), \\ \varphi'' &= \eta y'' \sin\varphi + \mathcal{M}(\varphi'), \end{aligned} \tag{3.203}$$

where

$$\begin{aligned} \zeta &= \frac{c}{\omega(M+m)}, \quad \gamma = \frac{d^2 k_2}{\omega^2(M+m)}, \quad \mu = \frac{m}{M+m}, \\ \eta &= \frac{md^2}{(J+md^2)}, \quad \mathcal{M}\left(\varphi'\right) = \frac{\mathcal{M}\left(\dot{\varphi}\right)}{\omega^2\left(J+m_2d^2\right)}, \end{aligned} \tag{3.204}$$

and $(') = d/d\tau$, $('') = d^2/d\tau^2$, ζ is the damping coefficient, γ is the nonlinear parameter of the potential, while μ and η are physical characteristics of the system. The torque is assumed to be linear, i.e.,

$$\mathcal{M}(\varphi') = E_1 - E_2\varphi', \tag{3.205}$$

with voltage or the strength of the motor E_1 and with characteristic parameter of the motor E_2. For (3.205) the equations of motion are

$$\begin{aligned} y'' + \zeta y' - y + \gamma y^3 &= \mu(\varphi'' \sin\varphi + \varphi'^2 \cos\varphi), \\ \varphi'' &= \eta y'' \sin\varphi + E_1 - E_2\varphi'. \end{aligned} \tag{3.206}$$

If this system has a principal parametric resonance 2:1, we assume that the oscillator vibrates with frequency Ω, but the frequency of non-ideal force is equal to $\Omega/2$. As the voltage source is alternated, E_1 is periodic and has the form

$$E_1 = u_0 \cos\left(\frac{\upsilon_0}{2}\tau\right), \tag{3.207}$$

where u_0 is the amplitude of the voltage source and $\upsilon_0 = \Omega/\omega$. Substituting (3.207) into (3.206) we obtain

$$\begin{aligned} y" + \zeta y' - y + \gamma y^3 &= \mu(\varphi" \sin\varphi + \varphi'^2 \cos\varphi), \\ \varphi" &= \eta y" \sin\varphi + u_0 \cos\left(\frac{\upsilon_0}{2}\tau\right) - E_2\varphi'. \end{aligned} \tag{3.208}$$

Due to the strong nonlinearity there is no exact analytical solution for (3.208). Let us assume the approximate solution in the form

$$\begin{aligned} y &= A_0 + A_1 \cos(\upsilon_0\tau) + A_2 \sin(\upsilon_0\tau), \\ \varphi &= B_0 + B_1 \cos\frac{(\upsilon_0\tau)}{2} + B_2 \sin\frac{(\upsilon_0\tau)}{2}, \end{aligned} \tag{3.209}$$

where A_0 is the amplitude of the structure, B_0 is the amplitude of the rotor at rest, $A = \sqrt{A_1^2 + A_2^2}$ is the amplitude of oscillator and $B = \sqrt{B_1^2 + B_2^2}$ is the rotor amplitude. To obtain approximate solutions we expand the nonlinear function $\sin\varphi$ and $\cos\varphi$ in the Taylor series until third order around the lower steady state for $\varphi = 0$. Substituting (3.209) into (3.208), balancing the harmonics and neglecting the derivatives of the second order and terms having derivatives in a power higher than one, the set of first order approximate differential equations follows as

$$\begin{aligned} 0 = {} & \zeta A_1' + 2\omega A_2' - \upsilon_0\mu(B_2B_1' + B_1B_2')\left(1 - \frac{B_1^2}{4} - \frac{B_2^2}{12} + \frac{5}{4}B_0^2\right) + \zeta\upsilon_0 A_2 \\ & + \left(-1 - \upsilon_0^2 + \frac{3}{4}\gamma(A_1^2 + A_2^2) + 3\gamma A_0^2\right) A_1 + \frac{\upsilon_0^2}{4}\mu\left(1 - \frac{B_0^2}{2}\right)(B_1^2 - B_2^2), \end{aligned}$$

$$\begin{aligned} 0 = {} & \gamma A_2' + 2\omega A_1' + \upsilon_0\mu(B_1B_1' - B_2B_2')\left(1 - \frac{B_1^2}{6} - \frac{B_0^2}{2}\right) - \zeta\upsilon_0 A_1 \\ & + \left(-1 - \upsilon_0^2 + \frac{3}{4}\gamma(A_1^2 + A_2^2) + 3\gamma A_0^2\right) A_2 + \frac{\upsilon_0^2}{2}\mu B_1 B_2\left(1 - \frac{B_0^2}{2}\right), \end{aligned}$$

$$
\begin{aligned}
0 = {} & \omega\varepsilon_2 B_2(A_1' + \frac{\upsilon_0}{2}A_2)\left(1 - \frac{B_1^2}{4} - \frac{B_2^2}{12} - \frac{B_0^2}{2}\right) + E_2 B_1' \\
& + \upsilon_0 B_2' + \frac{\upsilon_0}{2}E_2 B_1 - \frac{\upsilon_0^2}{4}B_1 - u_0 \\
& + \upsilon_0\eta(B_1 A_2' + \frac{\upsilon_0}{2}A_1 B_1)\left(1 - \frac{B_1^2}{6} - \frac{B_0^2}{2}\right),
\end{aligned}
$$

$$
\begin{aligned}
0 = {} & \upsilon_0\eta B_1(A_1' + \frac{\upsilon_0}{2}A_2)\left(1 - \frac{B_2^2}{4} - \frac{B_1^2}{12} - \frac{B_0^2}{2}\right) + E_2 B_2' \\
& - \upsilon_0 B_1' - \frac{\upsilon_0}{2}E_2 B_1 - \frac{\upsilon_0^2}{4}B_2 \\
& - \upsilon_0\eta(B_2 A_2' + \frac{\upsilon_0}{2}A_1 B_2)\left(1 + \frac{B_2^2}{6} - \frac{B_0^2}{2}\right),
\end{aligned}
$$

$$
\begin{aligned}
0 &= A_0\left(\frac{3}{2}\gamma(A_1^2 + A_2^2) + \gamma A_0^2 - 1\right), \\
0 &= \frac{\upsilon_0^2}{8}\eta B_0\left(A_1(B_2^2 - B_1^2) - 2A_2 B_1 B_2\right).
\end{aligned} \tag{3.210}
$$

Relations $(3.210)_5$ and $(3.210)_6$ are satisfied for

$$
\gamma A_0^2 = 1 - \frac{3}{2}\gamma A, \quad B_0 = 0. \tag{3.211}
$$

Besides, let us assume for small oscillations that $B^2 = 0$.Using this assumption and (3.211) the Eqs. $(3.210)_1$–$(3.210)_4$ give the steady states when

$$
A_1' = 0, \quad A_2' = 0, \quad B_1' = 0, \quad B_2' = 0,
$$

as

$$
\begin{aligned}
0 &= \zeta\upsilon_0 A_2 + \left(-1 - \upsilon_0^2 + \frac{3}{4}\gamma(A_1^2 + A_2^2) + 3\gamma A_0^2\right)A_1 + \frac{\upsilon_0^2}{4}\mu(B_1^2 - B_2^2), \\
0 &= -\zeta\upsilon_0 A_1 + \left(-1 - \upsilon_0^2 + \frac{3}{4}\gamma(A_1^2 + A_2^2) + 3\gamma A_0^2\right)A_2 + \frac{\upsilon_0^2}{2}\mu B_1 B_2, \\
u_0 &= \eta\frac{\upsilon_0^2}{2}(A_1 B_1 + A_2 B_2) + \frac{\upsilon_0}{2}E_2 B_2 - \frac{\upsilon_0^2}{4}B_1 - \eta\frac{\upsilon_0^2}{8}A_2 B_2 B_1^2, \\
0 &= -\eta B_1\frac{\upsilon_0^2}{8}A_2 B_2^2 - \frac{\upsilon_0}{2}E_2 B_1 - \frac{\upsilon_0^2}{4}B_2 - \eta\frac{\upsilon_0^2}{2}(A_1 B_2 - A_2 B_1).
\end{aligned} \tag{3.212}
$$

Equation (3.212) represent the set of four coupled equations. According to some specific considerations the system of Eq. (3.212) have semi-trivial and non-trivial solutions.

3.5.1 *Semi-trivial Solutions and Quenching of Amplitude*

The semi-trivial solution means physically that one part of the system is oscillating while the other one is at rest. This gives the condition for quenching of amplitude of oscillation of one part of the system: of the mechanical part and of the non-ideal force.

Quenching of amplitude in the mechanical part satisfies the following requirements

$$A_1 = A_2 = 0, \quad B_1 \neq 0, \quad B_2 \neq 0. \tag{3.213}$$

For these values the mechanical part of the system does not vibrate. This case can be used as a technique of control whose objective is to cancel vibration of the mechanical system. According to (3.210) the condition of quenching phenomenon in the space of the parameters of the system is derived and given as

$$B = \frac{2u_0}{\upsilon_0\sqrt{E_2^2 + (\frac{\upsilon_0}{2})^2}}. \tag{3.214}$$

In Fig. 3.28, the amplitude of non-ideal force B as function of the frequency υ_0, given with (3.211), is plotted. For numerical purposes, the following set of parameters (Souza et al. 2005a, b) is considered

$$\zeta = 0.02, \quad \gamma = 0.1, \quad \mu = 0.1, \quad \eta = 0.25, \quad E_2 = 1.5.$$

Analytical solution is compared with numerical solution of (3.210) using the fourth-order Runge Kutta algorithm (see Fig. 3.28).

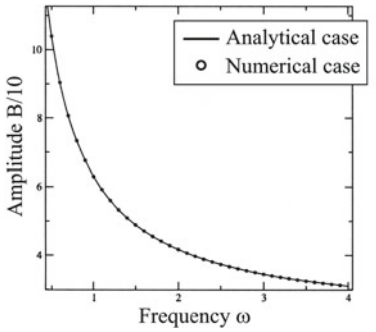

Fig. 3.28 Amplitude-frequency curve of non-ideal system for semi-trivial case. (Nbendjo et al. 2012)

It appears that the amplitude of the non-ideal force decreases as the frequency increases. To analyze the stability of this semi-trivial solution, the amplitude modulation equations are given by

$$\begin{aligned}\dot{A}_1 &= f_1(A_1, A_2, B_1, B_2),\\ \dot{A}_2 &= f_2(A_1, A_2, B_1, B_2),\\ \dot{B}_1 &= f_3(A_1, A_2, B_1, B_2),\\ \dot{B}_2 &= f_4(A_1, A_2, B_1, B_2).\end{aligned} \tag{3.215}$$

Perturbing the solution A_1, A_2, B_1 and B_2 with $\delta A_1, \delta A_2, \delta B_1$ and δB_2 and substituting into (3.215), after linearization a set of differential equations is obtained. Stability conditions are based on the eigenvalues of the Jacobian (Warminski and Kecik 2006). If the solution is complex, and the real part of the eigenvalue is always negative, the system is stable.

Quenching of amplitude of the non-ideal force occurs for

$$B_1 = 0, \quad B_2 = 0, \quad A_1 \neq 0, \quad A_2 \neq 0. \tag{3.216}$$

This situation represents the case where the non-ideal forces does not swing and the structure vibrates. Using the set of differential equations for steady-state motion (3.212) and assuming the stationarity of solutions leads after some calculations to the following non-linear equation of the amplitude

$$A = \sqrt{\frac{(\frac{15}{4}\gamma)^2 + \zeta^2 \upsilon_0^2 + (2 - \upsilon_0^2)^2}{\frac{15}{2}\gamma(2 - \upsilon_0^2)}}. \tag{3.217}$$

Analyzing of this equation shows the evidence of mechanical part which is at equilibrium and thus the system remains stable.

3.5.2 Non-trivial Solutions and Their Stability

Non-trivial solutions represent the case where both systems vibrate and

$$A_1 \neq 0, \quad A_2 \neq 0, \quad B_1 \neq 0, \quad B_2 \neq 0. \tag{3.218}$$

Analytically, we were supposed to use the set of Eq. (3.210) and to derive the amplitude of both systems. Unfortunately, the system is strongly nonlinear and it is quite impossible to obtain an analytical expression of amplitude.

Moreover, to deal with such a question, we solved directly the base equations (3.208) numerically using the fourth-order Runge–Kutta algorithm and discuss the amplitude resonance curves. Afterwards, we explore the stability of the system using

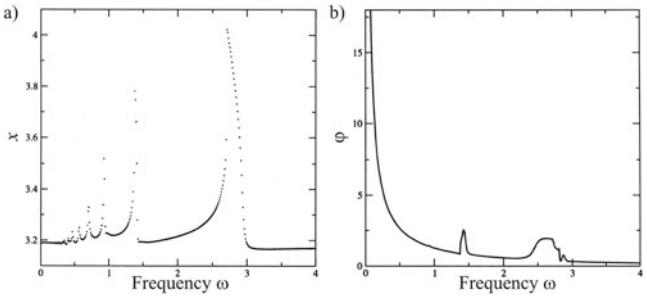

Fig. 3.29 **a** Amplitude of the mechanical part as function of the frequency; **b** Amplitude of the non-ideal source as function of the frequency (Nbendjo et al. 2012)

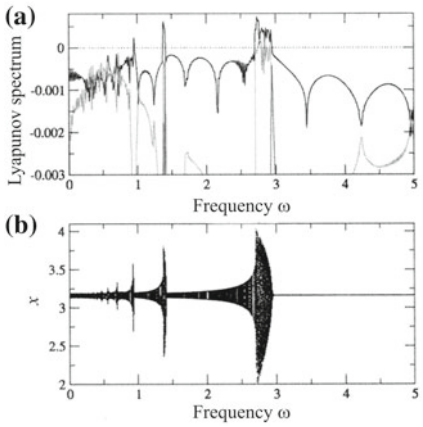

Fig. 3.30 **a** Lyapunov spectrum and **b** bifurcation diagram as function of υ_0 for $u_0 = 1$ (Nbendjo et al. 2012)

Lyapunov spectrum and bifurcation sequences. The frequency response curve is thus obtained from (3.208) and presented in Fig. 3.29a for the evaluation x and in Fig. 3.29b for evaluation of φ for $u_0 = 1$.

Figure 3.29a reveals a set of subharmonic resonances instead of the internal resonance 2:1 as expected. Concerning the amplitude of non-ideal forces, it decreases as frequency increases and the effect of internal resonance is visible by their appearance.

Focusing on the stability of the system allows one to display the Lyapunov spectrum as function of frequency for the specify value of $u_0 = 1$.

It appears, for example in Fig. 3.30a, that the Lyapunov spectrum is positive for certain values of frequency which is necessary for the presence of chaos in the system. On the other hand, for another set of frequencies, Fig. 3.30a shows more than one positive Lyapunov exponent, indicating hyperchaos on the system. These effects are confirmed via the corresponding bifurcation diagram (see Fig. 3.30b). Setting $\upsilon_0 = 1.5$ allows one to observe the stability of the system as u_0 increases.

It appears in Fig. 3.31a that the system shows a transient from periodicity to quasiperiodicity and later to chaos. To view how these transient arise, the corresponding

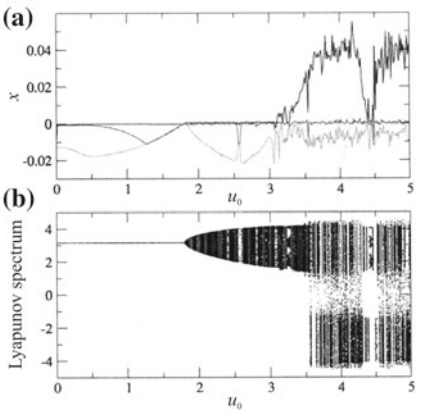

Fig. 3.31 Lyapunov spectrum and corresponding bifurcation diagram as function of u_0 for $\upsilon_0 = 1.5$ (Nbendjo et al. 2012)

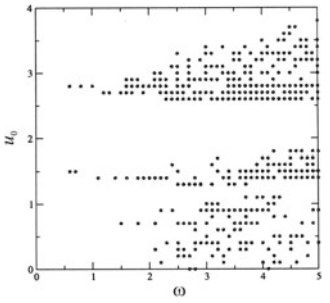

Fig. 3.32 Region in parameter space of (u_0, υ_0) where hyperchaos is detected (Nbendjo et al. 2012)

bifurcation diagram is presented in Fig. 3.31b, which confirms the results obtained from the Lyapunov spectrum. It shows that for $u_0 = 0.36$ there is a crisis in which sudden change in chaotic attractors occurs. Summarizing, it is concluded that there are regions in which all Lyapunov exponents are less or equal to zero for periodic or quasiperiodic orbits. If one of the Lyapunov exponents is positive, chaos is evident. If more than one positive Lyapunov spectrum exists, the presence of the hyperchaos for a specific set of parameters is indicated (Fig. 3.32).

Based on these consideration it can be concluded that the stability of the systems deeply depends on the voltage of the energy source.

3.5.3 Conclusion

Alternating strength of the voltage of the source may be the reason for the limited power supply for the bistable Duffing oscillator. Thus, in the oscillator - non-ideal source system for certain parameters quenching phenomena occurs: quenching of amplitude in the mechanical part or quenching of amplitude of the non-ideal force. Besides, in the system an explosion of resonances 2:1 to a set of subharmonic

resonances is revealed. Based on stability analysis of the non-trivial solutions we concluded that the periodicity of the voltage source perturbs the limited power supply and increases the possibility of the appearance of chaos and hyperchaos of the systems. Consequently, when the voltage source is alternated, if the choice of the characteristic is bad, the system can become unstable.

Appendix: Ateb Functions

Sine Ateb Function

The incomplete Beta function is defined as (see Abramowitz and Stegun 1964, 1979)

$$B_x(p,q) = \int_0^{0\le x\le 1} t^{p-1}(1-t)^{q-1}dt, \tag{A1}$$

while for the case $x = 1$, the complete Beta function is obtained

$$B(p,q) = \int_0^1 t^{p-1}(1-t)^{q-1}dt, \tag{A2}$$

where p and q are real numbers. For the positive integrands in (A1) and (A2), the interval for the incomplete beta function is

$$0 \le B_x(p,q) \le B(p,q). \tag{A3}$$

For the functions $B(p,q)$ and $B_x(p,q)$ the following identities are evident

$$B(p,q) = B(q,p), \quad B_x(p,q) = B(p,q) - B_y(p,q), \tag{A4}$$

where $x + y = 1$.

Let us determine the inverse of the half of the incomplete beta function (A1)

$$x \to \frac{1}{2}B_x(p,q) = \frac{1}{2}\int_0^{0\le x\le 1} t^{p-1}(1-t)^{q-1}dt. \tag{A5}$$

Introducing the notation (Cveticanin 2014)

$$\frac{1}{2}B_x(p,q) = w, \tag{A6}$$

the half of the incomplete beta function is

$$\frac{1}{2}\int_0^{0\le x\le 1} t^{p-1}(1-t)^{q-1}dt = w. \tag{A7}$$

For the the new variables

$$t = \bar{v}^{1/p}, \quad x = v^{1/p}, \tag{A8}$$

the boundary of integration $0 \le x \le 1$ transforms into $0 \le |v| \le 1$ and the integral (A7) has the forms

$$\frac{1}{2p}\int_0^{0\le v\le 1} (1-\bar{v}^{1/p})^{q-1}d\bar{v} = w, \quad \frac{1}{2p}\int_0^{-1\le v\le 0} (1-\bar{v}^{1/p})^{q-1}d\bar{v} = w. \tag{A9}$$

Let us consider the first integral in (A9). For $v = 0$ the integral is zero, and for $v = 1$ it is according to (A5)

$$\frac{1}{2p}\int_0^1 (1-\bar{v}^{1/p})^{q-1}d\bar{v} = \frac{1}{2}B(p,q). \tag{A10}$$

Thus, the value of the function w (A9) is bounded

$$0 \le w \le \frac{1}{2}B(p,q), \tag{A11}$$

as $B(p,q)$ is finite. Now, the inverse for the integral (A9) is constructed. This inverse depends on the three parameters p, q and w. With notation given by Rosenberg (1963, 1966) we have

$$v = sa\left(\frac{1-p}{p}, \frac{1-q}{q}, w\right), \tag{A12}$$

The second integral in (A9) gives

$$-v = sa\left(\frac{1-p}{p}, \frac{1-q}{q}, -w\right). \tag{A13}$$

It follows that $\mathrm{sa}(\frac{1-p}{p}, \frac{1-q}{q}, w)$ is the inverse of (A9) on the interval $-\frac{1}{2}B(p,q) \le w \le \frac{1}{2}B(p,q)$. Formula (A9) defines w uniquely as a function of v in this interval. Using the odd property (A13) of inverse of (A9), Rosenberg (1963) named the function 'sine Ateb function' and noted as sa.

The period of the function is

$$2\Pi(p,q) = 2B(p,q). \tag{A14}$$

Cosine Ateb Function

The change of variables

$$t = 1 - \bar{u}^{1/q}, \quad x = 1 - u^{1/q}, \tag{A15}$$

transforms the interval $0 \le x \le 1$ into $0 \le |u| \le 1$. Substituting (A15) into (A7), for $1 \ge u \ge 0$, it yields

$$-\frac{1}{2q}\int_{1}^{0\le u\le 1}(1-\bar{u}^{1/q})^{p-1}d\bar{u} = w. \tag{A16}$$

Due to the property of the beta function (A4), we have

$$-\frac{1}{2q}\int_{0}^{0\le u\le 1}(1-\bar{u}^{1/q})^{p-1}d\bar{u} + \frac{1}{2q}\int_{0}^{1}(1-\bar{v}^{1/q})^{p-1}d\bar{u} = w, \tag{A17}$$

i.e.,

$$-\frac{1}{2q}\int_{0}^{0\le u\le 1}(1-\bar{u}^{1/q})^{p-1}d\bar{u} = -\frac{1}{2}B(p,q) + w. \tag{A18}$$

Using the notation of the inverse function (A12) i.e. (A13) and the period $\Pi(p,q) = B(p,q)$ we obtain

$$u = \pm sa\left(\frac{1-q}{q}, \frac{1-p}{p}, \frac{1}{2}\Pi(p,q) \mp w\right). \tag{A19}$$

The inverse function u Rosenberg (1963) called 'cosine Ateb function' and noted it with ca:

$$ca\left(\frac{1-q}{q}, \frac{1-p}{p}, w\right) = sa\left(\frac{1-p}{p}, \frac{1-q}{q}, \frac{1}{2}\Pi(p,q) \pm w\right). \tag{A20}$$

The ca function is an even function (see Senik (1969a, b), Drogomirecka (1997)) with period $2\Pi(p,q)$ given with (A14).

Properties of Ateb Functions

The relation which satisfy the sa and the ca Ateb functions is (Gottlieb 2003, Gricik and Nazarkevich 2007)

$$\mathrm{sa}^2\left(\frac{1-p}{p},\frac{1-q}{q},w\right)+\mathrm{ca}^{\alpha+1}\left(\frac{1-q}{q},\frac{1-p}{p},w\right)=1. \tag{A21}$$

The first derivatives of sa and ca functions are

$$\frac{d}{dw}\mathrm{sa}\left(\frac{1-p}{p},\frac{1-q}{q},w\right)=\mathrm{ca}^{\alpha}\left(\frac{1-q}{q},\frac{1-p}{p},w\right), \tag{A22}$$

$$\frac{d}{dw}\mathrm{ca}\left(\frac{1-q}{q},\frac{1-p}{p},w\right)=-\frac{2}{\alpha+1}\mathrm{sa}\left(\frac{1-p}{p},\frac{1-q}{q},w\right). \tag{A23}$$

The Fourier series expansion of the ca Ateb function (Gricik et al. 2009) is as follows

$$\mathrm{ca}\left(\frac{1-q}{q},\frac{1-p}{p},w\right)=\sum_{n=1}^{\infty}a_n\cos\frac{\pi n w}{\Pi(p,q)}, \tag{A24}$$

where $a_0=0$ and

$$a_n=\frac{2}{\Pi(p,q)}\int_0^{\Pi(p,q)}\mathrm{ca}\left(\frac{1-q}{q},\frac{1-p}{p},w\right)\cos\frac{\pi n w}{\Pi(p,q)}dw. \tag{A25}$$

Namely, the coefficient is enough to be calculated for $w\in[0,\Pi(p,q)/2]$.

References

Abramowitz, M., & Stegun, I. A. (1964). *Handbook of mathematical functions*. National Bureu of Standards: Applied Mathematics Series, vol. 55. National Bureau of Standards, Washington.

Abramowitz, M., & Stegun, I. A. (1979). *Handbook of mathematical functions with formulas, graphs and mathematical tables*. Moscow: Nauka. (in Russian).

Amore, P., & Aranda, A. (2005). Improved Lindstedt-Poincaré method for the solution of nonlinear problems. *Journal of Sound and Vibration*, *283*, 1115–1136.

Andrianov, I. V. (2002). Asymptotics of nonlinear dynamical systems with high degree of nonlinearity. *Doklady RAN*, *386*, 165–168.

Andrianov, I. V., & Awrejcewicz, J. (2003a). Asymptotic approaches to strongly nonlinear dynamical systems. *Journal on Systems Analysis Modelling Simulation*, *43*, 255–268.

Andrianov, I. V., & Awrejcewicz, J. (2003b). Asymptotical behaviour of a system with damping and high power-form nonl-linearity. *Journal of Sound and Vibration*, *267*, 1169–1174.

Belendez, A., Pascual, C., Gallego, S., Ortuño, M., & Neipp, V. (2007). Application of a modified He's homotopy perturbation method to obtain higher-order approximations of an $x^{1/3}$ force nonlinear oscillator. *Physics Letters A*, *371*, 421–426.

Bogolyubov, N. N., & Mitropolskij, Ju A. (1974). *Asimptoticheskie metodi v teorii nelinejnih kolebanij*. Moscow: Nauka.

Castao, K. A. L., Goes, C. S., & Balthazar, J. M. (2010). A note on the attenuation of the sommerfeld effect of a non-ideal system taking into account a MR damper and the complete model of a DC motor. *Journal of Vibration and Control*, *17*(7), 1112–1118.

Chen, S. H., & Cheung, Y. K. (1996). An elliptic perturbation method for certain strongly non-linear oscillators. *Journal of Sound and Vibration*, *192*, 453–464.

Chen, W. H., & Gibson, R. F. (1998). Property distribution determination for nonuniform composite beams from vibration response measurements and Galerkin's method. *Journal of Applied Mechanics, ASME*, *65*, 127–133.

Chen, S. H., Yang, X. M., & Cheung, Y. K. (1998). Periodic solutions of strongly quadratic nonlinear oscillators by the elliptic perturbation method. *Journal of Sound and Vibration*, *212*, 771–780.

Cheng, Y. K., Chen, S. H., & Lau, S. L. (1991). A modified Lindstedt-Poincaré method for certain strongly non-linear oscillators. *International Journal of Nonlinear Mechanics*, *26*, 367–378.

Colm, I. J., & Clark, N. J. (1988). *Forming, shaping and working of high-performace ceramics*. New York: Blackie.

Cveticanin, L. (1992). An approximate solution for a system of two coupled differential equations. *Journal of Sound and Vibration*, *153*, 375–380.

Cveticanin, L. (1993). An asymptotic solution to weak nonlinear vibrations of the rotor. *Mechanism and Machine Theory*, *28*, 495–506.

Cveticanin, L. (1995). Resonant vibrations of nonlinear rotors. *Mechanism and Machine Theory*, *30*, 581–588.

Cveticanin, L. (2003). Vibrations of the system with quadratic non-linearity and a constant excitation force. *Journal of Sound and Vibration*, *261*(1), 169–176.

Cveticanin, L. (2004). Vibrations of the nonlinear oscillator with quadratic nonlinearity. *Physica A*, *341*, 123–135.

Cveticanin, L. (2006). Homotopy-perturbation method for pure non-linear differential equation. *Chaos, Solitons and Fractals*, *30*, 1221–1230.

Cveticanin, L. (2008). Analysis of oscillators with non-polynomial damping terms. *Journal of Sound and Vibration*, *317*, 866–882.

Cveticanin, L. (2009). Oscillator with fraction order restoring force. *Journal of Sound and Vibration*, *320*, 1064–1077.

Cveticanin, L. (2011). Pure odd-order oscillators with constant excitation. *Journal of Sound and Vibration*, *330*, 976–986.

Cveticanin, L. (2014). On the truly nonlinear oscillator with positive and negative damping. *Applied Mathematics and Computation*, *243*, 433–445.

Cveticanin, L., & Pogany, T. (2012). Oscillator with a sum of non-integer order non-linearities. *Journal of Applied Mathematics*, Article ID 649050, 20 p. doi:10.1155/2012/649050.

Cveticanin, L., & Zukovic, M. (2015a). Non-ideal mechanical system with an oscillator with rational nonlinearity. *Journal of Vibration and Control*, *21*(11), 2149–2164.

Cveticanin, L., & Zukovic, M. (2015b). Motion of a motor-structure non-ideal system. *European Journal of Mechanics A/Solids*, *53*, 229–240 (2015_2).

Cveticanin, L., Kalami-Yazdi, M., Saadatnia, Z., & Askari, H. (2010). Application of hamiltonian approach to the generalized nonlinear oscillator with fractional power. *International Journal of Nonlinear Sciences and Numerical Simulation*, *11*, 997–1002. ($(2010)_1$).

Cveticanin, L., Kovacic, I., & Rakaric, Z. (2010). Asymptotic methods for vibrations of the pure-non-integer order oscillator. *Computers and Mathematics with Applications*, *60*, 2616–2628.

Cveticanin, L., Kalami-Yazdi, M., & Askari, H. (2012). Analytical approximations to the solutions for a generalized oscillator with strong nonlinear terms. *Journal of Engineering Mathematics*, *77*(1), 211–223.

Dantas, M. H., & Balthazar, J. M. (2003). On the appearance of a Hopf bifurcation in a non-ideal mechanical system. *Mechanics Research Communications*, *30*, 493–503.
Dantas, M. H., & Balthazar, J. M. (2006). A comment on a non-ideal centrifugal vibrator machine behavior with soft and hard springs. *International Journal of Bifurcation and Chaos*, *16*, 1083–1088.
Dantas, M. J. H., & Balthazar, J. M. (2007). On the existence and stability of periodic orbits in non ideal problems: General results. *Zeitschrift fur angewandte Mathematik und Physik*, *58*, 940–958.
Dimentberg, M. F., McGovern, L., Norton, R. L., Chapdelaine, J., & Harrison, R. (1997). Dynamics of an unbalanced shaft interacting with a limited power supply. *Nonlinear Dynamics*, *13*, 171–187.
Drogomirecka, H. T. (1997). Integrating a special Ateb-function. *Visnik Lvivskogo Universitetu. Serija mehaniko-matematichna*, *46*, 108–110. (in Ukrainian).
Droniuk, I. M., Nazarkevich, M. A., & Thir, V. (2010). Evaluation of results of modelling Ateb-functions for information protection. *Visnik nacionaljnogo universitetu Lvivska politehnika*, *663*, 112–126. (in Ukrainian).
Droniuk, I., & Nazarkevich, M. (2010). Modeling nonlinear oscillatory system under disturbance by means of Ateb-functions for the Internet. *Proceedings of the 6th International working Conference on Performance Modeling and Evaluation of Heterogeneous Networks (HET-NETs'10), Zakopane, Poland* (pp. 325–334).
Droniuk, I. M., Nazarkevich, M. A., & Thir, V. (1997). Evaluation of results of modelling Ateb-functions for information protection. Visnik Nacionaljnogo Universitatu Lvivskogo Universitetu. *Serija Mehanika-matematichna*, *46*, 108–110.
Fang, T., & Dowell, E. H. (1987). Numerical simulations of periodic and chaotic responses in a stable Duffing system. *International Journal of Non-Linear Mechanics*, *22*, 401–425.
Felix, J. L. P., Balthazar, J. M., & Dantas, M. J. H. (2009a). On energy pumping, synchronization and beat phenomenon in a nonideal structure coupled to an essentially nonlinear oscillator. *Nonlineaer Dynamics*, *56*, 1–11.
Felix, J. L., Balthazar, J. M., & Brasil, R. M. L. R. F. (2009b). Comments on nonlinear dynamics of a non-ideal Duffing-Rayleigh oscillator: Numerical and analytical approaches. *Journal of Sound and Vibration*, *319*, 1136–1149.
Gendelman, O., & Vakakis, A. F. (2000). Transitions from localization to nonlocalization in strongly nonlinear damped oscillators. *Chaos, Solitons and Fractals*, *11*, 1535–1542.
Gottlieb, H. P. W. (2003). Frequencies of oscillators with fractional-power non-linearities. *Journal of Sound and Vibration*, *261*, 557–566.
Gradstein, I. S., & Rjizhik, I. M. (1971). *Tablicji integralov, summ, rjadov i proizvedenij*. Moscow: Nauka.
Gricik, V. V., & Nazarkevich, M. A. (2007). Mathematical models algorythms and computation of Ateb-functions. *Dopovidi NAN Ukraini Seriji A*, *12*, 37–43. (in Ukrainian).
Gricik, V. V., Dronyuk, I. M., & Nazarkevich, M. A. (2009). Document protection information technologies by means of Ateb-functions I. Ateb-function base consistency for document protection. *Problemy upravleniya i avtomatiki*, *2*, 139–152. (in Ukrainian).
Haslach, H. W. (1985). Post-buckling behavior of columns with non-linear constitutive equations. *International Journal of Non-Linear Mechanics*, *20*, 53–67.
Haslach, H. W. (1992). Influence of adsorbed moisture on the elastic post-buckling behavior of columns made of non-linear hydrophilic polymers. *International Journal of Non-Linear Mechanics*, *27*, 527–546.
He, J.-H. (2002). Modified Lindstedt-Poincaré methods for some strongly non-linear oscillations Part I: Expansion of a constant. *International Journal of Non-Linear Mechancis*, *37*, 309–314.
http://functions.wolfram.com/GammaBetaErf/Beta3/26/01/02/0001 (2002a).
http://functions.wolfram.com/HypergeometricFunctions/Hypergeometric2F1/03/09/19/02/0017 (2002b).
http://functions.wolfram.com/EllipticIntegrals/EllipticF/16/01/02/0001 (2002c).
http://functions.wolfram.com/EllipticFunctions/Hypergeometric2F1/03/07/17/01/0012 (2002d).
http://functions.wolfram.com/EllipticFunctions/JacobiAmplitude/16/01/01/0001.

Hu, H., & Xiong, Z. G. (2003). Oscillations in an $x^{(2m+2)/(2n+1)}$ potential. *Journal of Sound and Vibration*, *259*, 977–980.

Jutte, C. V. (2008). Generalized synthesis methodology of nonlinear springs for prescribed load-displacement functions. Ph.D. Dissertation, Mechanical Engineering, The University of Michigan.

Kononenko, V. O. (1969). *Vibrating system with a limited power supply*. London: Illife.

Kononenko, V. O., & Korablev, S. S. (1959). An experimental investigation of the resonance phenomena with a centrifugal excited alternating force. *Trudji Moskovskog Teknichkog Instutita*, *14*, 224–232.

Kovacic, I., Rakaric, Z., & Cveticanin, L. (2010). A non-simultaneous variational approach for the oscillators with fractional-order power nonlinearity. *Applied Mathematics and Computation*, *217*, 3944–3954.

Krylov, N., & Bogolubov, N. (1943). *Introduction to nonlinear mechanics*. New Jersey: Princeton University Press.

Lewis, G., & Monasa, F. (1982). Large deflections of a cantilever beams of nonlinear materials of the Ludwick type subjected to an end moment. *International Journal of Non-Linear Mechancis*, *17*, 1–6.

Lo, C. C., & Gupta, S. D. (1978). Bending of a nonlinear rectangular beam in large deflection. *Journal of Applied Mechanics, ASME*, *45*, 213–215.

Lyapunov, A. M. (1893). An investigation of one of the singular cases of the theory of the stability of motion. *II Mathematicheski Sbornik*, *17*, 253–333. (in Russian).

Mickens, R. E. (2001). Oscillations in an $x^{4/3}$ potential. *Journal of Sound and Vibration*, *246*, 375–378.

Mickens, R. E. (2004). *Mathematical methods for the natural and engineering sciences*. New Jersey: World Scientific.

Mickens, R. E. (2006). Iteration method solutions for conservative and limit-cycle $x^{1/3}$ force oscillators. *Journal of Sound and Vibration*, *292*, 964–968.

Nayfeh, A. H., & Mook, D. T. (1979). *Nonlinear oscillations*. New York: Wiley.

Nbendjo, B. R. N., Caldas, I. L., & Viana, R. L. (2012). Dynamical changes from harmonic vibrations of a limited power supply driving a Duffing oscillator. *Nonlinear Dynamics*, *70*(1), 401–407.

Ozis, T., & Yildirm, T. A. (2007). Determination of periodic solution for a $u^{1/3}$ force by He's modified Lindstedt-Poincaré method. *Journal of Sound and Vibration*, *301*, 415–419.

Patten, W. N., Sha, S., & Mo, C. (1998). A vibration model of open celled polyurethane foam automative seat cuchions. *Journal of Sound and Vibration*, *217*, 145–161.

Pezeshki, C., & Dowell, E. H. (1988). On chaos and fractal behaviour in a general Duffing's system. *Physica D*, *32*, 194–209.

Pilipchuk, V. N. (2010). *Nonlinear dynamics: Between linear and impact limits*. New York: Springer.

Prathap, G., & Varadan, T. K. (1976). The inelastic large deformation of beams. *ASME Journal of Applied Mechanics*, *43*, 689–690.

Pyragas, K. (1992). Continuous control of chaos by self controlling feedback. *Physics Letters A*, *170*, 421–428.

Pyragas, K. (1995). Control of chaos via extended delay feedback. *Physics Letters A*, *206*, 323–330.

Rosenberg, R. M. (1963). The ateb(h)-functions and their properties. *Quarterly of Applied Mathematics*, *21*, 37–47.

Rosenberg, R. M. (1966). On nonlinear vibrating systems with many degrees of freedom. *Advances in Applied Mechanics*, *32*, 155–242.

Russell, D., & Rossing, T. (1998). Testing the nonlinearity of piano hammers using residual shock spectra. *Acta Acustica*, *84*, 967–975.

Senik, P. M. (1969a). Inversion of the incomplete beta function. *Ukrainski Matematicheskii Zhurnal*, *21*, 271–278.

Senik, P. M. (1969b). Inversion of the incomplete Beta-function. *Ukrainski matematicheski zhurnal 21, 325-333 and Ukrainian Mathematical Journal*, *21*, 271–278.

Souza, S. L. T., Caldas, I. L., Viana, R. L., Balthazar, J. M., & Brasil, R. M. L. R. F. (2005a). Impact dampers for controlling chaos in systems with limited power supply. *Journal of Sound and Vibration*, *279*, 955–965.

Souza, S. L. T., Caldas, I. L., Viana, R. L., Balthazar, J. M., & Brasil, R. M. L. R. F. (2005b). Basins of attraction changes by amplitude constraining of oscillators with limited power supply. *Chaos, Solitons and Fractals*, *26*, 1211–1220.

Tsuchida, M., Guilherme, K. L., Balthazar, J. M., & Silva, G. N., (2003). On regular and irregular vibrations of a non-ideal system with two degrees of freedom. 1:1 resonance. *Journal of Sound and Vibration*, *260*, 949–960.

Tsuchida, M., Guilherme, K. L., & Balthazar, J. M. (2005). On chaotic vibrations of a non-ideal system with two degree of freedom. 1:2 resonance and Sommerfeld effect. *Journal of Sound and Vibration*, *282*, 1201–1207.

Ueda, Y. (1985). Random phenomena resulting from non-linearity in the system described by Duffing's equation. *International Journal of Non-Linear Mechanics*, *20*, 481–491.

Van Dooren, R., & Janssen, H. (1996). A continuation algorithm for discovering new chaotic motions in forced Duffing systems. *Journal of Computational and Applied Mathematics*, *66*, 527–541.

Warminski, J., & Kecik, K. (2006). Autoparametric vibrations of a nonlinear system with pendulum. Mathematical Problems in Engineering (No 80705).

Warminski, J., Balthazar, J. M., & Brasil, R. M. L. R. F. (2001). Vibrations of a non-ideal parametrically and self-excited model. *Journal of Sound and Vibration*, *245*, 363–374.

Wolf, A., Swift, J., Swinney, H., & Vastano, J. (1985). Determining Lyapunov exponents from a time series. *Physica D*, *16*, 285–317.

Yuste, S. B., & Bejarano, J. D. (1986). Construction of approximate analytical solution to a new class of a non-linear oscillator equations. *Journal of Sound and Vibration*, *110*, 347–350.

Yuste, S. B., & Bejarano, J. D. (1990). Improvement of a Krylov-Bogolubov method that uses Jacobi elliptic functions. *Journal of Sound and Vibration*, *139*, 151–163.

Zhuravlev, V. F., & Klimov, D. M. (1988). *Applied methods in oscillation theory*. Moscow: Nauka.

Zukovic, M., & Cveticanin, L. (2007). Chaotic responses in a stable Duffing system on non-ideal type. *Journal of Vibration and Control*, *13*, 751–767.

Zukovic, M., & Cveticanin, L. (2009). Chaos in non-ideal mechanical system with clearance. *Journal of Vibration and Control*, *15*, 1229–1246.